Structural and Functional Analysis of the RANTES-Glycosaminoglycans Interactions†

Loïc Martin,‡,§ Cédric Blanpain,‡,|| Pascale Garnier,§ Valérie Wittamer,|| Marc Parmentier,|| and Claudio Vita*,§

CEA (Commissariat à l'Energie Atomique) Saclay, Département d'Ingénierie et d'Etudes des Protéines, F-91191 Gif-sur-Yvette, France, and IRIBHN (Institut de Recherche Interdisciplinaire en Biologie Humaine et Nucléaire), Université Libre de Bruxelles, Campus Erasme, 8-1070 Bruxelles, Belgium

Received November 20, 2000; Revised Manuscript Received March 13, 2001

ABSTRACT: Chemokines mediate their biological activity through activation of G protein coupled receptors, but most chemokines, including RANTES, are also able to bind glycosaminoglycans (GAGs). Here, we have investigated, by site-directed mutagenesis and chemical acetylation, the role of RANTES basic residues in the interaction with GAGs using surface plasmon resonance kinetic analysis. Our results indicate that (i) RANTES exhibited selectivity in GAGs binding with highest affinity (K_d = 32.1 nM) for heparin, (ii) RANTES uses the side chains of residues R44, K45, and R47 for heparin binding, and blocking these residues in combination abolished heparin binding. The biological relevance of RANTES−GAGs interaction was investigated in CHO−K1 cells expressing CCR5, CCR1, or CCR3 and the various GAGs that bind RANTES. Our results indicate that the heparin binding site, defined as the 40s loop, is only marginally involved in CCR5 binding and activation, but largely overlaps the CCR1 and CCR3 binding and activation domain in RANTES. In addition, enzymatic removal of cell surface GAGs by glycosidases did not affect CCR5 binding and Ca^{2+} response. Furthermore, addition of soluble GAGs inhibited both CCR5 binding and functional response, with a rank of potency similar to that found in surface plasmon resonance experiments. Thus, cell surface GAGs is not a prerequisite for receptor binding or signaling, but soluble GAGs can inhibit the binding and the functional response of RANTES to CCR5 expressing cells. However, the marked selectivity of RANTES for different GAGs may serve, in vivo, to control the concentration of specific chemokines in inflammatory situations and locations.

Chemokines are small size (∼8.0 kDa) chemotactic cytokines that play a critical role in immunosurveillance and inflammation by controlling activation and migration of specific leukocytes (*1*−*4*). Chemokines are related in sequence and, on the basis of a conserved cysteine motif near to the N-terminus, have been classified in four different families. CC or β chemokines (MIP-1α, MIP-1β, RANTES,[1] MCP-1, MCP-2, MCP-3, ...) constitute the largest family and are characterized by the presence of two contiguous cysteine residues near their N-terminus. The CXC or α chemokine family (Il-8, IP-10, NAP-2, PF-4, ...) is characterized by the presence of two cysteine residues nearest to the N-terminus separated by one residue. The other two C and CX3C chemokine families contain only one member each, the C chemokine lymphotactin (*5*), presenting a single cysteine near to the N-terminus, and the CX3C chemokine fractalkine (*6*), presenting three amino acid residues separating the first two cysteine residues. Chemokines present a similar basic structural motif formed by an N-terminal unstructured segment followed by a triple stranded β-sheet, arranged in a greek key motif and crossed by a C-terminal α-helix (Figure 1). While some chemokines are monomeric at physiological concentrations (e.g., MCP-1 and SDF-1α), most of them are able to associate in dimers, tetramers or higher order polymers.

The biological activity of chemokines is mediated via seven-transmembrane-helix receptors, coupled to G-proteins, present predominantly in leukocytes (*1*−*4*). Upon binding to the cell receptor, chemokines stimulate intracellular calcium and chemotaxis in target leukocytes. However, a CC chemokine can usually bind several receptors, and most chemokine receptors (CCR) can be activated by different chemokines. In addition, chemokines play also an important

† This work was supported by the French Agence Nationale de Recherche sur le SIDA (ANRS) to C.V. and M.P., and by the Actions de Recherche Concertées of the Communauté Française de Belgique, the Centre de Recherche Inter-universitaire en Vaccinologie, the Belgian program on Interuniversity Poles of attraction initiated by the Belgian State, Prime Minister's Office, Science Policy Programming, the BIOMED and BIOTECH programs of the European Community (Grants BIO4-CT98-0543 and BMH4-CT98-2343), the Fonds de la Recherche Scientifique Médicale of Belgium and the Fondation Médicale Reine Elisabeth to M. P. C. B. is Aspirant of the Belgian Fonds National de la Recherche Scientifique and V.W. is fellow of the Fond d'Encouragement à la Recherche dans l'Industrie et l'Agriculture.

* To whom correspondence should be addressed. Phone: (+33) 169087133. Fax: (+33) 169089071. E-mail: claudio.vita@cea.fr.

‡ LM and CB contributed equally to this work.

§ CEA.

|| IRIBHN.

[1] Abbreviations: Alloc, allyloxycarbonyl; CSA, chondroitin sulfate A.; CSC, chondroitin sulfate C; Dde, 1-(4,4-dimethyl-2,6-dioxocyclohex-1-ylidene)ethyl; DS, dermatan sulfate; GAGs, glycosaminoglycans; Hep, heparin; HS, heparan sulfate; MIP, macrophage inflammatory protein; Mtt, 4-methyltrityl; RANTES, regulated on activation normal T-cell expressed; RU, response unit.

10.1021/bi002670n CCC: $20.00
Published on Web 05/04/2001

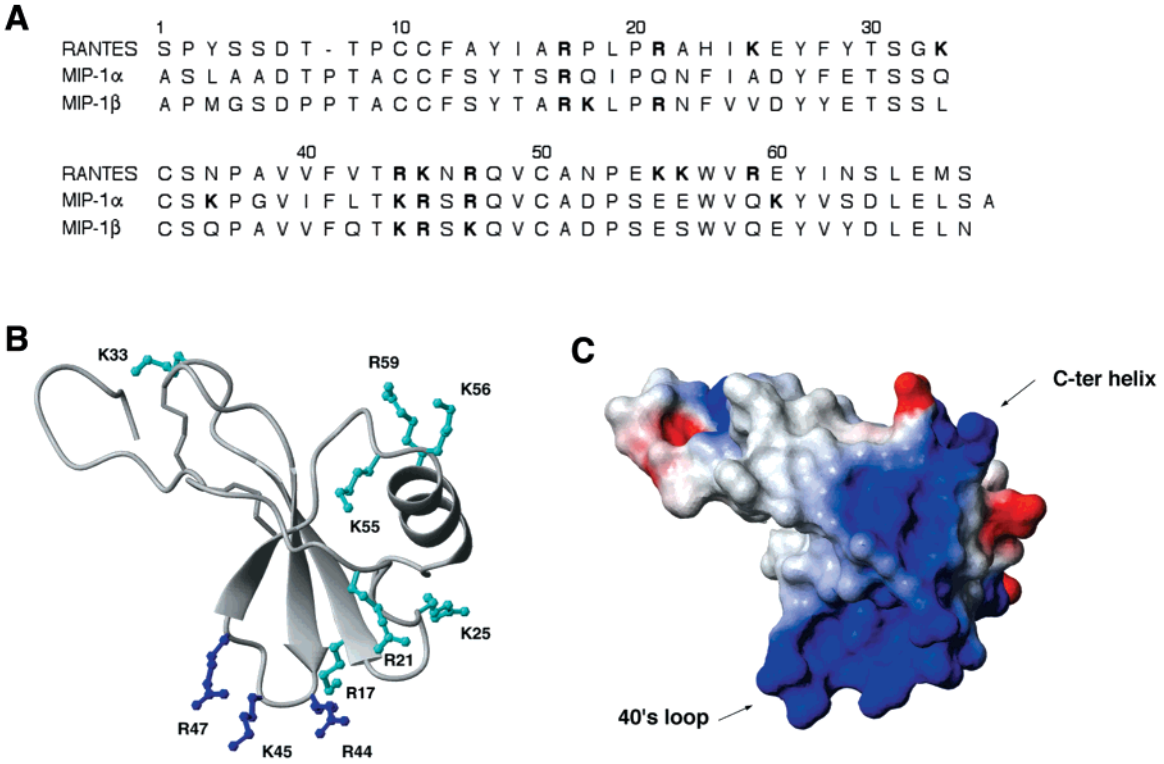

FIGURE 1: Amino acid sequence alignment (A) of RANTES, MIP-1α, MIP-1*β* and three-dimensional model (B, C) of RANTES. (A) Basic residues in RANTES, MIP-1α and MIP-1*β* sequence are in bold. (B) Structural model [Molmol representation (*48*)] of RANTES monomer (1hrj, PDB code) emphasizing the side chains acetylated in the current study. Side chains of 40s loop, R44, K45, and R47, are in blue. Other basic side chains are in cyan. (C) Electrostatic surface potential (Molmol representation) of RANTES monomer (oriented as in panel B), showing two regions of positively charged residues, centered about the 40s loop and C-terminal helix region. Positive or negative potential is in blue or red, respectively.

suppressive role in AIDS progression. For example, CC chemokine RANTES, MIP-1α, and MIP-1*β* can protect cell from infection by the macrophage tropic HIV-1 strains, that use CCR5 as co-receptors for entry (*7*).

The biological activity of chemokines has been shown to be critically influenced by their association with glycosaminoglycans (GAGs) (*8*, *9*), tethered to the serine residue of proteoglycans on the cellular surface and extracellular matrix. GAGs are highly sulfated oligosaccharides, which are posttranslationally and heterogeneously sulfated by membrane-bound specific enzymes (*10*). The most common GAGs are heparin (Hep), heparan sulfate (HS), chondroitin sulfate A and C (CSA, CSC), dermatan sulfate (DS) and hyaluronic acid (HA). Chemokines have been shown to be stored and released from T lymphocytes cytolytic granules complexed to GAGs (*11*). In addition, MIP-1*β* bound to tissue matrix GAGs has been shown to induce adhesion of T-cells to endothelium (*12*). These observations suggest that interaction with matrix and endothelium GAGs may help to create a gradient of chemokines immobilized on GAGs and direct migration of leukocytes. GAG binding has also been shown to influence chemokine structure and promote aggregation in vitro (*13*). GAG induced aggregation may also increase local concentration of chemokines and increase their in vivo half-life, thus protecting them from degradation. However, recent and sometimes conflicting results have suggested that GAGs might have even more important roles in chemokine function. Indeed, cell surface GAGs have been reported to facilitate binding of chemokines to their receptors (*13*) and their removal by glycosidases resulted in loss of intracellular Ca^{2+} mobilization. (*14*).

Binding of chemokines to GAGs is essentially determined by electrostatic interaction (*18*) between the positively charged basic residues (arginine and lysine) of the chemokine and the negatively charged sulfate and carboxylate groups of GAGs. The molecular interaction of chemokines with different GAGs has been addressed in a number of studies. The basic C-terminal α-helix of Il-8 (*16*, *17*), PF-4 (*18*) and MCP-1 (*19*) have been identified as the region involved in GAG binding. The CC chemokines MIP-1α and MIP-1*β* do not have a basic C-terminal α-helix (Figure 1), so a different region should be responsible for GAG binding. In two independent studies (*20*, *21*), residues K45, R46, and R48 or residues R18, R46, and R48 of MIP-1α were shown to be essential to heparin binding. In addition, residues R18, K45, and R46 of the structurally homologous chemokine MIP-1*β* have been shown to be critical for GAG binding (*22*). These residues identified an exposed loop in MIP-1*β* and MIP-1α, which is spatially remote from the C-terminal α-helix. Furthermore, a recent study demonstrates that the CXC chemokine SDF-1α associates to heparin through the first *β*-strand, involving the basic residues K24, H25, and K27 (*23*). Thus, no general structural features characterize GAG binding for all chemokines. RANTES presents basic residues at 20s strand, 40s loop, and C-terminal α-helix (Figure 1).

The purpose of this work is to investigate the nature of RANTES interacting with GAGs and the role of GAG interaction in RANTES function. By using an optimized chemical synthesis protocol, we have produced RANTES derivatives in which all the side chains of the basic residues have been blocked, one by one, by acetylation. These charge

neutralization mutants were analyzed by plasmon resonance biosensor kinetic analysis, CCR5 and CCR1 binding and CCR5, CCR1, and CCR3 Ca^{2+} release tests. Our results indicate that RANTES uses the side chains of residues R44, K45, and R47 for heparin binding, with R47 playing a dominant role. However, the heparin binding site is only marginally involved in CCR5 binding and activation, while overlaps the CCR1 and CCR3 binding and activation domains. Interestingly, suppression of GAG binding did not result in decrease of RANTES function, indicating that GAG binding is not necessary for biological activity. In addition, enzymatic removal of cellular GAGs did not affect either CCR5 binding or Ca^{2+} response, while addition of soluble GAGs was always inhibitory in both CCR5 binding and functional response. RANTES showed large differences in binding affinity for different GAGs, with a marked preference for heparin. This selectivity in GAG-binding may have an important role in vivo, since the composition of cell surface GAGs may control both the type of chemokine and the formation of concentration gradient in inflammatory situations and loci.

EXPERIMENTAL PROCEDURES

Materials. All Fmoc-protected amino acids and *N*,*N*′-dicyclohexylcarbodiimide were from Nova Biochem (Laufelfingen, Switzerland), except Fmoc-Lys(Alloc), which was from Neosystem (Strasbourg, France). 1-*N*-Hydroxy-7-azabenzotriazole (HOAt) was from Perseptive Biosystems (PE Biosystems France). All other reagents and solvents used in the synthesis and purification were from Fluka (St. Quentin Fallavier, France) or SDS (Peypin, France). Pioneer chip F1, the amine coupling kit containing *N*-hydroxy-succinimide (NHS), *N*-ethyl-*N*′-[(diethylamino)propyl] carbodiimide (EDC) and surfactant P20 (Tween 20) were obtained from Biacore (Uppsala, Sweden). Heparin (13.5−15.0 kDa) was from Calbiochem (Meudon, France), while all other glycosaminoglycans, chondroitin sulfate A (45.5 kDa), chondroitin sulfate C, dermatan sulfate (37 kDa), dextran sulfate (5.0 kDa), and heparan sulfate (7.5 kDa), were from Sigma.

All HPLC analyses were performed with a Spectra-Physics system (ThermoQuest, Les Ulis, France), consisting of a P2000 pump, UV 3000 detector, controlled by a PC computer. All HPLC purifications were performed on a Jasco system (Jasco, Nantes, France), consisting of two PU-956 pumps, a UV-975 detector and Merck-Hitachi D7500 Integrator.

Chemical Synthesis. RANTES and RANTES analogues were synthesized on an Applied Biosystems Synthesizer model 433A by the solid-phase method, by using fluorenylmethyloxycarbonyl (Fmoc)-amino acid derivatives and 1-*N*-hydroxy-7-azabenzotriazole (HOAt)/*N*,*N*′-dicyclohexylcarbodiimide (DCCI) mediated coupling. Amino acid side chain blocking groups were *tert*-butyl ether for Ser, Thr, Tyr; *tert*-butyl ester for Asp, Glu; 2,2,5,7,8-pentamethylchroman-6-sulfonyl for Arg; trityl for Asn, Cys, His, and Gln. Particular lysine side chains were protected by the following orthogonal protecting groups, 1-(4,4 dimethyl-2,6-dioxocyclohex-1-ylidene)ethyl (Dde), 4-methyltrityl (Mtt), allyloxycarbonyl (Alloc); common lysine side chains were protected by *tert*-butyloxycarbonyl (t-Boc). N-Amino terminal serine was incorporated as BocSer(tBu) and with 2-(1-*H*-benzotriazol-1-yl)-1,1,3,3-tetramethyluronium hexafluorophosphate (HBTU) coupling. Syntheses started with 50 μmol of the C-terminal Fmoc-Ser(*tert*-butyl) covalently attached to the hydroxymethylphenoxy polystyrene resin (HMP-resin, 0.65 mmol/g, Applied Biosystems), and the polypeptide chain was assembled by coupling 1 mmol of Fmoc-amino acid derivatives (20-fold molar excess) for 30 min in *N*-methylpyrrolidone (NMP), followed by 10 min capping with acetic anhydride. Fmoc-protection was removed by three 3 min treatments with 20% piperidine in NMP. UV-monitoring (at 301 nm) of deprotection cycles was then used to add deprotection cycles until deprotection was complete and to extend coupling time (up to 50 min), in the case of difficult deprotection. All acetylated RANTES derivatives were obtained in four syntheses, by using the following lysine orthogonal protecting groups: synthesis 1, K55(Alloc), K56-(Mtt), K59(Dde); synthesis 2, K44(Alloc), K45(Mtt), K47-(Dde); synthesis 3, K21(Mtt), K33(Dde); synthesis 4, K17-(Alloc), K25(Mtt), K56(Dde). After completion of chain assembly, orthogonal protecting groups on lysine side chains were individually removed and freed ϵ-amino groups acetylated as outlined below. Dde was removed by three treatments with 2% hydrazine in DMF for 3 min. Mtt was deprotected by eight successive 5 min treatments with 1% trifluoroacetic acid (TFA) in dichloromethane (DCM). Alloc deprotection was performed in nitrogen atmosphere directly into the reaction vessel of the ABI 433A synthesizer by a protocol specifically set up for this reaction, based on the published chemistry (*24*). Briefly, the peptide-resin (12.5 μmol) was vortexed, in the synthesizer reactor vessel, with a mixture of the borane ammonia complex (10 molar excess, Aldrich) dissolved in 2.5 mL of NMP, and of tetrakis-(triphenyl phosphine) Pd(0) (0.1 M equiv, Aldrich) dissolved in 1.0 mL of DCM and 1.0 mL of NMP, for 30 min; the resin was then washed by NMP, and the deprotection procedure repeated once more. Acetylation was manually performed with acetic anhydride (5%, v/v), diisopropylethylamine (DIEA, 6%, v/v) in dimethylformamide. Finally, the peptides were cleaved from the resin with simultaneous removal of side-chain protective groups by treatment with Reagent K (82.5% trifluoacetic acid, 5% water, 5% phenol, 5% thioanisole, and 2.5% ethanedithiol) for 2 h at room temperature. The resin was then filtered off and the fully deprotected peptide was precipitated in methyl-*tert*-butyl ether at 4 °C. After centrifugation and washing three times with ether, the peptide was dissolved in 20% acetic acid and lyophilized.

Purification. The crude reduced product was purified by reversed-phase HPLC on a Vydac C_4 column (2.5 × 25 cm) eluted at 15 mL/min flowrate with a 50 min linear 25 to 50% acetonitrile gradient in 0.1% aqueous trifluoroacetic acid. Fractions from the major peak were analyzed on a Vydac C4 column (0.46 × 25 cm): single peak fractions were collected and lyophilized. Disulfide bonds were formed by dissolving the reduced purified proteins in a solution of 50 mM sodium phosphate buffer, pH 7.8, containing 2 M urea (cyanate free), 5 mM oxidized glutathione, and 0.5 mM reduced glutathione. After 2 h at room temperature, the oxidation solution was acidified to pH 3.0 with acetic acid and loaded directly on a Vydac C_4 column (2.5 × 25 cm) at 10 mL/min flow rate. The oxidized protein was then eluted using a linear 15 to 35% acetonitrile gradient in 0.1%

aqueous trifluoroacetic acid over 90 min at 15 mL/min flow rate. Eluted materials were analyzed by HPLC and capillary electrophoresis: >95% pure fractions were collected and lyophilized. Identity of purified products was verified by amino acid analysis and electrospray mass spectrometry.

Chemical Characterization. Amino acid analysis of hydrolyzed products (in 6 N HCl at 120 °C for 17 h) were analyzed on an Applied Biosystems 130A automatic Amino Acid Analyzer. Molecular masses were determined on a Quattro II triple quadropole (Micromass, Manchester, U.K.) equipped with an electrospray source. Data were analyzed with the manifacturer Masslynx software.

Analytical Ultracentrifugation. Sedimentation equilibrium analyses were performed at 20 °C on a Beckman Optima XLA analytical ultracentrifuge, using an AN 60 rotor and cell with a 12 mm optical path length. Sample volume of 100 μL were centrifuged at 9000, 15 000, 20 000, 30 000, and 40 000 rpm. Protein solutions were at 3.2−4.0 μM concentration, in 20 mM phosphate buffer, pH 7.2, containing either 0.15 M NaCl or 0.5 M NaCl. Radial scans of absorbance at 210 nm were taken at 3 h intervals. It was concluded that equilibrium has been achieved when no difference was observed between two scans recorded at 3 h interval. The final solute distribution data were analyzed by using the programs XL-A/KL-I Data Analysis supplied by Beckman. The partial specific volume was taken as 0.726 $cm^3\ g^{-1}$ and the solvent density 1.0188 g cm^{-3}.

Gel Filtration. Gel filtration experiments were performed using a SMART system apparatus equipped with a Superdex 75 PC 3.2/30 column (Pharmacia, Uppsala, Sweden), which was equilibrated and eluted with 20 mM sodium phosphate, 500 mM NaCl, pH 7.4, at a flow rate of 80 μL/min, with monitoring at 214 and 280 nm. A total of 50 μL of the various derivatives were injected at a concentration of 10 μM. Molecular weight standards (Sigma) were bovine serum albumin (BSA, 68 kDa), chymotrypsin (25 kDa), sperm whale myoglobin (17.8 kDa), horse heart cytochrome *c* (12.6 kDa), and aprotinin (6 kDa).

Biosensor Assays. Optical biosensor experiments were performed with a Biacore 2000 System (Biacore, Uppsala, Sweden) and a heparin sensorchip, obtained by immobilizing biotinylated-heparin on streptavidin F1 sensorchip. Biotinylated-heparin was prepared as follows: heparin (Calbiochem) (13 mg/mL) was first oxidized with sodium *m*-periodate (10 mM in 0.1 M sodium acetate, pH 5.5, for 1 h at room temperature), then reacted with biotinamidocaproylhydrazide (17 mM, overnight at room temperature). Derivatized heparin was purified on a Hi-trap desalting column (Pharmacia; column buffer: 10 mM Hepes, 300 mM NaCl, pH 7.4). Streptavidin was immobilized on F1 sensorchip as follows: sensorchip surface was first activated by injecting 50 μL of the amine coupling agent [*N*-ethyl-N′-(dimethylaminopropyl) carbodiimide (EDC)/N-hydroxysuccinimide (NHS), 0.2 M/0.05 M]; then, 20 μL of streptavidin (0.2 mg/mL in 10 mM sodium acetate, pH 4.5) were injected at a flowrate of 5 μL/min, followed by 4 × 20 μL of ethylenediamine 1.0 M (pH 8.5). Biotinylated-heparin (5 μg/mL in Hepes buffer saline−10 mM Hepes buffer, pH 7.4, containing 0.3 M NaCl) was then injected, at 10 μL/min flowrate, to two channels of the streptavidin-coated sensorchip to a RU value of 100 and 200, respectively (a third channel was not loaded and used as negative control). In a typical analysis, analytes at different concentrations were flowed onto the heparin-coated surface at a rate of 50 μL/min, at 25 °C and for a 3 min association time, after which the channels were rinsed with the running buffer (10 mM Hepes, 150 mM NaCl, 3.4 mM EDTA, and 0.05% P20, pH 7.4) to analyze the dissociation phase. After each experiment, the heparinized biosensor surface was regenerated with 25 μL of 1.0 M NaCl. Affinities were calculated from rate constants determined by the Bia-evaluation 3.0 software.

Cell Cultures. CHO−K1 cells expressing apoaequorin and CCR5 were cultured using HAM's F12 medium supplemented with 10% Fetal Calf Serum (Life Technologies), 100 units/mL penicillin, 100 μg/mL streptomycin (Life Technologies), 250 μg/mL zeocin (Invitrogen), and 400 μg/mL G418 (Life Technologies).

Chemokine Receptor Binding Assays. RANTES mutants were analyzed in competition binding experiments using CHO−K1 cell lines expressing CCR5 or CCR1, as previously described (*25*). Briefly, 40 000 cells (for CCR5) or 1 μg of membrane proteins (for CCR1) were incubated, for 90 min at 27 °C, with 0.08 nM [^{125}I]MIP-1β or [^{125}I]MIP-1α (2000 Ci/mmol, Amersham-Pharmacia) and variable concentrations of competitor. The bound tracer was separated by filtration through GF/B filters presoaked in 1% BSA. Filters were counted in β-scintillation counter. Binding parameters were analyzed with the PRISM software (GraphPad Software) using nonlinear regression applied to a one-site competition model. Competition binding with glycosydase-treated cells was performed as described above with cells (resuspended at a concentration of 4 × 10^6 cells/mL in binding buffer) that were preincubated with 1.0 UI/mL of heparinase (EC 4.2.2.7, Sigma), 0.01 UI/mL of heparinitase I (EC 4.2.2.8, Seikagaku), or 0.1 UI/mL of chondroitinase ABC (EC 4.2.2.4, Seikagaku) or a combination of the three enzymes for 1 h at 37 °C. Competition binding experiments with soluble GAGs were performed as described above with the exception that 0.1 nM of [^{125}I]RANTES (2000 Ci/mmol, Amersham-Pharmacia) was used as tracer and that the GF/B filters were presoaked in 0.3% PEI. Heparin, heparan sulfate, chondroitin sulfate A, and chondroitin sulfate C were tested for their inhibitory effect on [^{125}I]RANTES binding and the results were analyzed by nonlinear regression applied to a one-site competition model using the GraphPad PRISM software.

Analysis of Cell Surface Expression of Heparan-Sulfate. Heparan sulfate glycosaminoglycans present at the cell surface of CHO cell lines were quantified by FACS using an anti-heparan sulfate monoclonal antibody (HepSS-1 mAb, Seikagaku). Cells resuspended in DMEM/F12 (Life Technologies) at 5 × 10^6 cells/mL, were incubated or not with glycosidases for 1 h at 37 °C, washed with 3 mL of cold PBS and incubated for 30 min with 2 μg of anti-HS mAb in 100 μL of PBS containing 0.1% sodium azide and 0.1% BSA (FACS buffer). The cells were washed with 3.0 mL cold FACS buffer, incubated with a FITC labeled anti-mouse IgM monoclonal antibody for 30 min at 4 °C, and washed again with 3.0 mL of cold FACS buffer. Cell fluorescence was analyzed using FASCAN (Becton-Dickinson) and CellQuest software (Becton-Dickinson).

Chemokine Receptor Functional Assays. The functional response of chemokine receptors to the various RANTES mutants was analyzed by measuring the luminescence of

aequorin as described (*26*). CHO−K1 cells coexpressing CCR5, CCR1 or CCR3, apo-aequorin, and $G_{\alpha 16}$ resuspended at 5×10^6 cell/mL in DMEM/F12 were incubated in dark for 4 h with 5 μM of coelenterazine H (Molecular Probes). Before use, the cells were diluted 5-fold and 50 μL of cell suspension were added to 50 μL of medium containing the chemokines and the luminescence was measured for 30 s in a EG&G-Berthold luminometer. Functional parameters were analyzed with the GraphPad PRISM software using nonlinear regression applied to a sigmoidal dose−response model. The effect of heparinase, heparitinase I and chondroitinase ABC treatment of cells on their functional response to RANTES was tested by preincubating the CCR5 expressing cells with the enzymes as described above.

The effect of soluble GAGs on the functional response to different agonists was performed with the same functional assay. Different concentrations of GAGs were incubated with 20 nM RANTES, 20 nM [E66A] RANTES, 100 nM [Ac44−47] RANTES, 100 nM CCK, 20 μM ATP or 0.1% Triton X-100 in DMEM/F12 for 1 h at 4 °C. A total of 50 μL of a cell suspension was then added to 50 μL of the agonist-GAG mixture and the luminescence was measured for 30 s in a EG&G-Berthold luminometer.

RESULTS

Synthesis of RANTES Derivatives Acetylated at Basic Residues. RANTES contains 10 basic amino acid residues, R17, R21, K25, K33, R44, K45, R47, K55, K56, and R59 (Figure 1), which in physiological conditions carry positively charged groups at side chains, potentially interacting with GAGs negatively charged functions (sulfate and carboxylate). Each of these positive charges was neutralized one by one. Charge neutralization of the five lysine residues was achieved by acetylation of its side chain amino group. The five arginine residues were mutated into lysine, one by one (in the working hypothesis that this mutation did not change GAG affinity significantly), and subsequently individually acetylated at its ϵ-amino groups. Acetylation of a particular lysine side chain was achieved by using, during chemical synthesis, a lysine derivative carrying an N-ϵ-protecting group which is orthogonal to all other protecting groups; this strategy allowed, after completion of the synthesis, specific deprotection of a particular lysine side chain and subsequent acetylation. Furthermore, by using three different orthogonal protecting groups (see Experimental Procedures) for three particular lysine side chains in one synthesis, we prepared all 10 RANTES monoacetylated derivatives by performing four syntheses only. This strategy also allowed the obtainment of a double acetylated derivative, [Ac44−47]RANTES, utilizing the same peptide-resin used for the obtainment of monoacetylated derivatives at positions 44, 45, and 47. Folding of RANTES and RANTES derivatives was performed in the presence of 2.0 M urea and reduced/oxidized glutathione: the former was required to prevent the formation of precipitate during folding and the later to accelerate the oxidation process which, on the basis of HPLC analysis, was apparently complete in less than 10 min. Highly pure (>95%) RANTES derivatives were obtained by HPLC purification of the reduced form and subsequently of the oxidized (disulfide bridged) form. Folded RANTES and RANTES derivatives presented 4 ± 0.5 Da lower molecular mass, consistent with the formation of two disulfide bonds in the purified molecules. Yields in pure proteins were quite variable: while native RANTES and acetylated derivative at positions 17, 25, and 33 were obtained in 10−20% overall yields, some derivatives acetylated at lysine residues close to the C-terminus were obtained in 1.0% total yields only.

Effect of Neutralization of Positively Charged Residues of RANTES on Its State of Aggregation. As revealed by analytical ultracentrifugation experiments, RANTES, dissolved at relatively high 1−10 μM protein concentration and 0.15 M sodium chloride concentration, behaves as a high molecular mass aggregate (100−200 kDa, Figure 2A) (*27*). However, aggregation is reversible and we found that protein dilution and the presence of high sodium chloride concentration reduce aggregation of RANTES in solution. Thus, in the presence of 0.5 M sodium chloride and at the same 1−10 μM protein concentration, RANTES is a dimer (Figure 2B), in equilibrium with a monomer and a tetramer species. However, we found that neutralization of charged residues by acetylation affects RANTES aggregation. Indeed, acetylation of R44K has a disaggregating effect on RANTES, and in ultracentrifugation experiments, [Ac44]RANTES derivative, dissolved in the 1−10 μM protein concentration range and in the presence of only 0.15 M sodium chloride, is a dimer (Figure 2C). Since analytical ultracentrifugation is a quite involved technique and requires sophisticated instrumentation, we decided to use gel filtration technique to routinely monitor the aggregation state of RANTES and RANTES derivatives. We found that RANTES could be satisfactorily eluted in gel filtration columns only when at least 0.5 M NaCl salt was included in the column eluting buffer. At lower 0.15 M sodium chloride concentration, only a low percentage of the protein injected could be eluted. Thus, in the presence of 0.5 M sodium chloride and injected at a concentration not exceeding 1 μM, RANTES is eluted as a narrow peak at a volume corresponding to a dimer. However, injected at 10 μM or higher concentrations, RANTES is eluted as a broader peak, spanning a larger elution volume (Figure 2D). Mutation of RANTES E-66 was reported to reduce the tendency of the chemokine to aggregate (*27*). Thus, we synthesized the mutant [E66A]-RANTES, as a reference nonaggregating RANTES mutant. In fact, this mutant, injected in a wide concentration range (0.1−100 μM), was eluted from the column as a narrow peak and as a dimer (Figure 2D). As expected, also [Ac44]-RANTES was eluted as a sharp peak and as a dimer (Figure 2E). All acetylated RANTES derivatives were analyzed in gel filtration at 10 μM, and compared to wt RANTES (aggregated form) or [E66A]RANTES and [Ac44]RANTES (disaggregated forms) to monitor their aggregation state. In gel filtration, RANTES acetylated derivatives behave differently, depending on the position of the acetylation (Figure 2, panels E and F). Thus, RANTES derivatives acetylated at positions 17, 45, 47, and 55 were eluted as narrow peaks (Figure 2E). In contrast, derivatives acetylated at positions 21, 25, 33, 56, and 59 were eluted as broad peaks (Figure 2F) similarly to native aggregating RANTES. Thus, gel filtration experiments indicated that acetylation of RANTES residues R17K, R44K, K45, R47K, and K55 reduced the chemokine tendency to aggregation, while acetylation at R21K, K25, K33, K56, and R59K maintained the aggregation tendency of RANTES. Our data have been confirmed by tryptophan fluorescence polarization experiments and fluo-

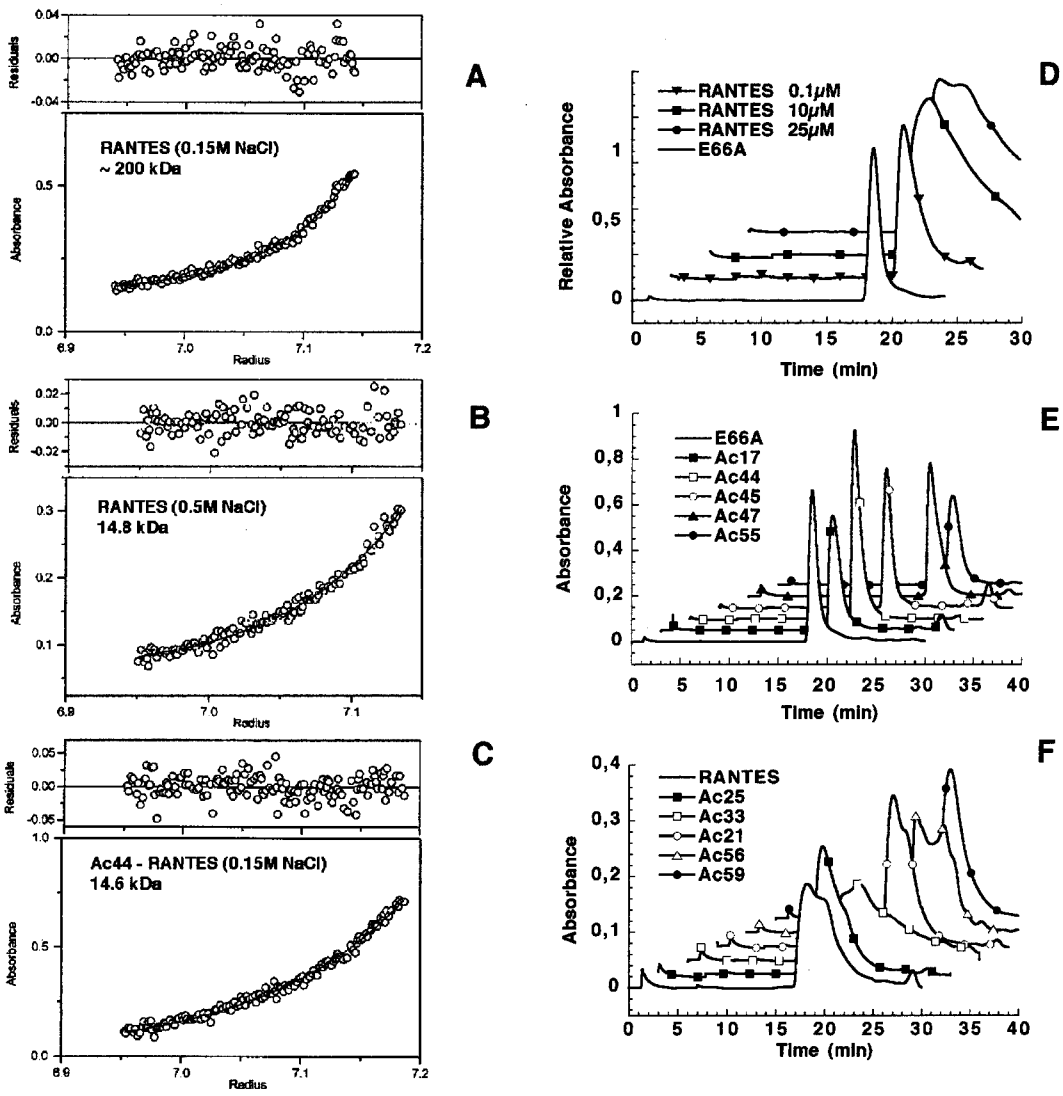

FIGURE 2: State of aggregation of RANTES and RANTES derivatives. Sedimentation equilibrium in analytical ultracentrifugation of RANTES (A, B), [Ac44]RANTES (C). Protein samples were dissolved at 4.0 μM (A), 3.0 μM (B), and 3.6 μM (C) concentration in 20 mM sodium phosphate buffer, pH 7.2, containing either 0.15 M (A, C) or 0.5 M NaCl (B). Absorbance was read at 210 nm. The solid line represents the best fit of the solute distribution data. Weight average molecular masses are shown. Gel filtration of RANTES (D), injected at 1.0, 10 and 25 μM concentration, [E66A]RANTES and acetylated RANTES derivatives (E, F), injected at 10 μM concentration. A Superdex 75 column was used and elution was performed with 20 mM sodium phosphate buffer, pH 7.4, containing 0.5 M NaCl, at a flow rate of 80 μL/min and with monitoring at 214 nm. Note that absorbance values in panel D have been arbitrary scaled up to the same value of 1.0 to better visualize the broadening effect due to aggregation.

rescence anisotropy determinations (not shown), and are in agreement with those reported by Czaplewski et al. (*27*). In particular, in gel filtration experiments [Ac33]RANTES was eluted as a very broad peak, suggesting that this derivative could present an increased tendency to aggregation.

Interaction of RANTES with GAGs by Biosensor Technology. We used the optical biosensor technology based on surface plasmon resonance (SPR) to analyze the RANTES−heparin interaction, its specificity for different GAGs and the effects of acetylation on heparin interaction. This technique measures real-time binding of soluble RANTES analyte to heparin ligand, immobilized on a dextran derivatized sensor chip surface. Detection is achieved by measuring refractive index changes near the sensor chip by plasmon resonance technology, as the consequence of protein interacting with the sensor chip surface. These changes in SPR angles are measured in response units (RU) and are directly correlated to the mass changes linked to the amount of protein bound at the sensor surface. Biotinylated heparin was immobilized at 100 RU on sensor chip, through noncovalent specific interaction with streptavidin, which was covalently bound to the dextran gel of the biosensor surfaces. When a RANTES solution was injected into biosensor flow cells and flowed over heparin surfaces for 180 s, a typical increase of the SPR response (in RU) vs time was obtained, corresponding to the association phase, which was then followed (180−550 s) by a decrease of SPR response, the dissociation phase, when the chemokine was replaced by running buffer (Figure 3A). When RANTES was flowed over control surfaces (containing streptavidin only) no significant signal (no binding) was observed (not shown). RANTES was flowed at 50 μL/min to minimize mass transport problems and at different concentrations in the range 0−400 nM; saturation was achieved at 400 nM, corresponding to 800 RU. The association and dissociation phase of the obtained sensorgrams could be fitted to the single Langmuir (A + B = AB)

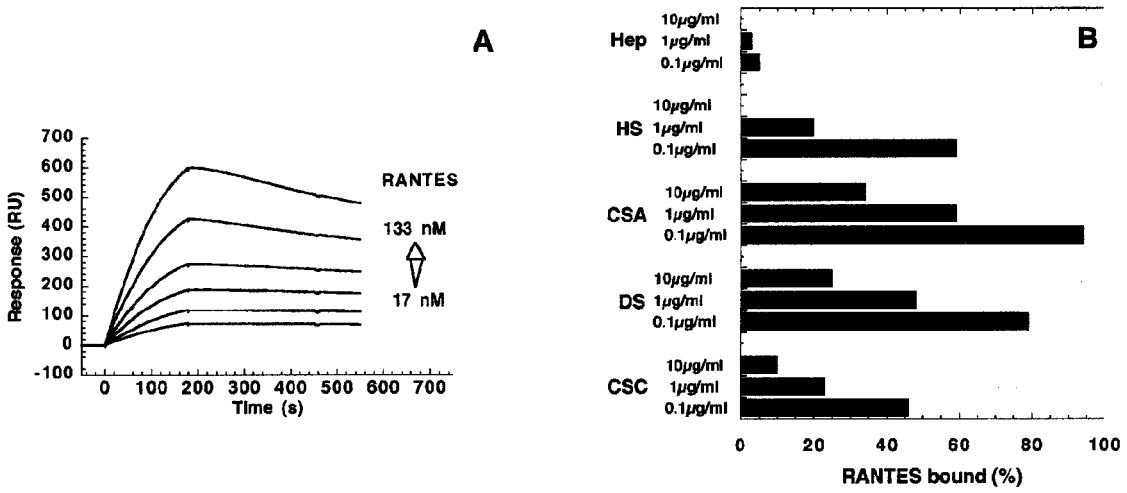

FIGURE 3: Surface plasmon resonance (SPR) analysis of RANTES/GAGs interaction. (A) Sensorgram overlay of RANTES binding to immobilized heparin. RANTES was injected over heparin-sensorchip (surface density 100 RU) at 17, 28, 39, 59, 88, and 133 nM concentration for 3 min (0−180 s) at 50 μL/min flow rate, followed by running buffer for 6 min. The RU response was recorded as a function of time and kinetic rates were calculated from both association and dissociation phases. (B) Inhibition of RANTES binding to heparin-sensorchip by GAGs. RANTES was incubated with heparin (Hep), heparan sulfate (HS), chondroitin sulfate A (CSA), dermatan sulfate (DS), chondroitin sulfate C (CSC) at 0.1, 1.0, and 10 μg/mL and then injected for 3 min on biosensor chips. Equilibrium RU responses were compared to maximum response in absence of GAG competitor and reported as percentages of RANTES bound.

Table 1: Summary of Binding and Functional Parameters of RANTES and RANTES Derivatives on Heparin and CCR5[a]

	heparin			CCR5	
name	k_{on} (10^4 $M^{-1}s^{-1}$)	k_{off} (10^{-3} s^{-1})	K_d (nM)	pIC_{50}	pEC_{50}
RANTES	5.3 ± 0.4	1.7 ± 0.5	32 ± 8	10.02 ± 0.12	8.76 ± 0.22
Ac17	6.2 ± 0.5	1.7 ± 0.3	27 ± 6	9.94 ± 0.04	8.23 ± 0.16
K17	11 ± 1	1.7 ± 0.4	15 ± 6	9.61 ± 0.10	8.22 ± 0.27
Ac21	7.1 ± 1.0	1.2 ± 0.4	18 ± 10	10.04 ± 0.16	8.56 ± 0.11
Ac25	3.3 ± 0.4	0.72 ± 0.05	22 ± 10	10.15 ± 0.16	8.67 ± 0.10
Ac33	5.2 ± 2.0	1.2 ± 0.3	24 ± 10	8.79 ± 0.19	7.28 ± 0.17
Ac44	1.4 ± 0.3	11 ± 8	785 ± 230	10.27 ± 0.22	8.84 ± 0.21
Ac45	0.76 ± 0.05	8 ± 5	1052 ± 548	9.98 ± 0.13	8.55 ± 0.20
Ac47	0.31 ± 0.06	11 ± 3	3550 ± 1000	9.91 ± 0.11	8.35 ± 0.17
Ac44−47	ND	ND	>100 μM	9.46 ± 0.01	7.64 ± 0.33
K44−47	19 ± 10	6.5 ± 0.5	34 ± 2	9.88 ± 0.05	8.30 ± 0.32
Ac55	4.1 ± 0.2	1.1 ± 0.7	27 ± 5	9.60 ± 0.17	8.13 ± 0.14
Ac56	5.2 ± 0.3	1.0 ± 0.5	20 ± 6	9.92 ± 0.17	8.76 ± 0.16
Ac59	6.4 ± 0.9	2.7 ± 0.6	43 ± 10	9.70 ± 0.03	8.68 ± 0.25

[a] The kinetic rate constants, k_{on}, k_{off}, and dissociation constants, $K_d = k_{on}/k_{off}$, of RANTES and [Ac47]RANTES were obtained by global analysis of association and dissociation phases in optical biosensor experiments at 17−133 nM and 59−1600 nM, respectively (as displayed in Figure 3A and 4C). Kinetic rate and dissociation constants for the other RANTES derivatives are the mean of data from three determinations. The pIC_{50} values were obtained from competition binding experiments, using 0.08 nM of [^{125}I]MIP-1β as tracer (as displayed in Figure 5). The pEC_{50} were obtained from functional dose−response curves using the aequorin assay (as displayed in Figure 6). Values represent the mean and sem of at least two independent determinations. One representative experiment is displayed in Figures 5 and 6.

model and analyzed by nonlinear fitting by Bia-evaluation version 3.0 software (see Experimental Procedures). Global fitting of binding curves gave an association rate constant (k_{on}) of 5.3 ± 0.4 10^4 M^{-1} s^{-1} and a dissociation rate constant (k_{off}) of 1.7 ± 0.5 10^{-3} s^{-1}. Thus, binding of RANTES to heparin is characterized by a dissociation constant ($K_d = k_{off}/k_{on}$) of 32.1 nM (Table 1). To examine the RANTES binding specificity for GAG, competition binding assays were performed. Thus, 100 nM RANTES solutions were incubated in the presence of different solution concentrations of GAGs and then injected on heparinized biosensor flow cells. Heparin was the most effective GAG in inhibiting RANTES binding to heparin bound to biosensor chip, with an apparent 50% of inhibition of binding (IC_{50}) of 25 ng/mL. Then, lower inhibiting efficacy is shown by chondroitin sulfate C (IC_{50} = 50 ng/mL), heparan sulfate (IC_{50} = 150 ng/mL), dermatan sulfate (IC_{50} = 800 ng/mL) and chondroitin sulfate A (IC_{50} = 8 μg/mL) (Figure 3B). Dextran sulfate also showed relatively high affinity (IC_{50} = 0.2 μg/mL), while mucin showed rather low affinity (IC_{50} = 30 μg/mL) and mannan was inactive (not shown). Heparin disaccharide I-s and chondroitin sulfate disaccharide II-s, as well as sialic acid, phytic acid, sucrose octasulfate were inactive at 10 μg/mL (not shown). Furthermore, since 100 RU of heparin (13.5−15.0 kDa) could bind to a maximum of 800 RU, the number of RANTES (7.8 kDa) molecules that bind to heparin could be estimated. This calculation results in 14−15 RANTES molecules bound per heparin molecule or one RANTES bound to 3.5 saccharide units.

Identification of RANTES Residues Interacting with GAGs. Using the same optical biosensor technology, we then examined the effect of acetylation of RANTES charged residues on heparin binding affinity. Monoacetylated RANTES derivatives were injected into heparinized biosensor flow

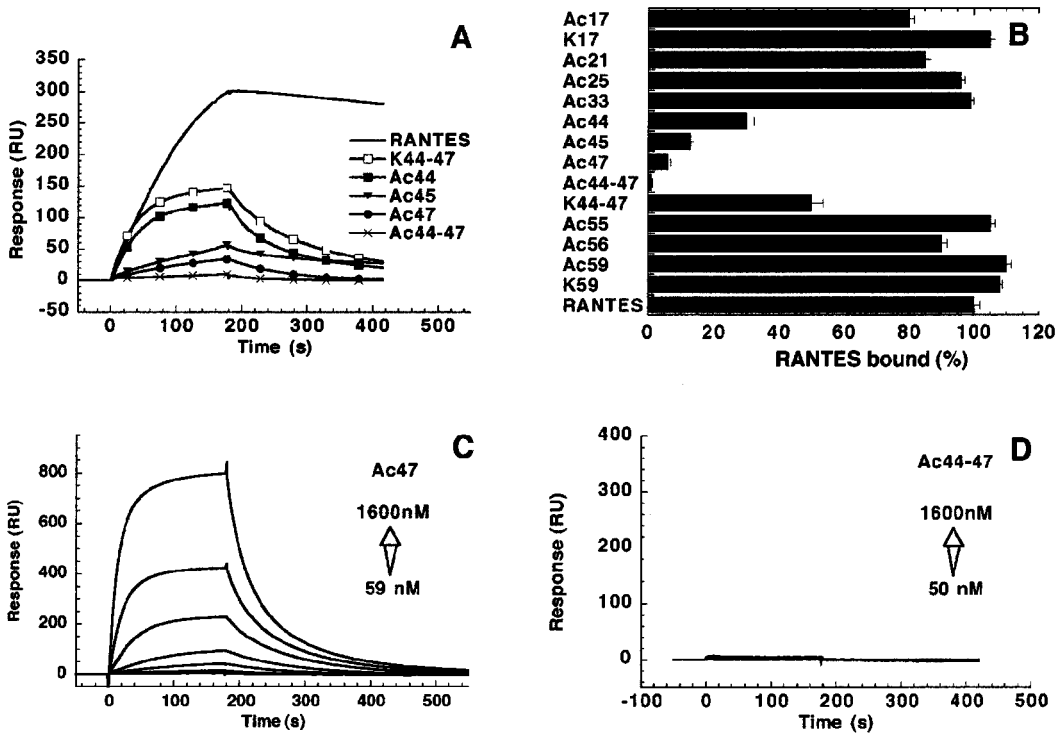

FIGURE 4: Effect of neutralization of RANTES positive charges on GAGs binding. (A) Surface plasmon resonance (SPR) sensorgrams of RANTES, [Ac44]RANTES, [Ac45]RANTES, [Ac47]RANTES, [Ac44−47]RANTES, and [K44−47]RANTES binding to immobilized heparin. Chemokine solutions were injected over heparin-sensorchip (surface density 100 RU) at 100 nM concentration. (B) Binding of RANTES mutants to heparin-sensorchips. Each chemokine was injected at 100 nM and 200 nM for 3 min and the equilibrium binding RU responses were reported as percentages of RANTES response. Sensorgram overlay of [Ac47]RANTES (C) (injected at 59, 88, 133, 200, 400, 800, and 1600 nM) and [Ac44−47]RANTES (D) (injected at 50, 100, 200, 400, 800, and 1600 nM) binding to heparin immobilized on sensor chips.

cells at 100 nM and their maximum RU signals were compared to that observed with RANTES. Acetylation of R44K, K45, and R47K resulted in derivatives with the maximum reduction of optical biosensor signal; [Ac47]-RANTES being the most affected (Figure 4A). Derivatives acetylated at positions 21, 25, 33, 55, 56, and 59 did not present significant difference in maximum signal, while [Ac17]RANTES showed only 20% RU signal decrease compared to RANTES (Figure 4B). Not acetylated R17K, R21K, and R59K RANTES mutants produced maximum signal similar to wt RANTES, while R44K and R47K mutants showed a reduction in signal not exceeding 20% of wt RANTES signal. To obtain a relative estimate of heparin binding affinity of all acetylated derivatives, individual sensorgrams were then fitted to a 1:1 binding model and results are reported in Table 1. This analysis clearly demonstrates that only acetylation of positions 44, 45, 47, affects RANTES binding affinity for heparin, while acetylation of all other positions did not produce significant changes in heparin binding affinity. A complete kinetic study of [Ac47]RANTES binding to heparin was also performed by injecting this derivative in the concentration range 0−1.6 μM (Figure 4C). To obtain a set of sensorgrams from which association and dissociation phases could be analyzed, we injected this derivative over the biosensor surfaces in range of concentration (0−1.6 μM) higher than that previously used with wt RANTES. By global fitting of the association and dissociation phase of the obtained sensorgrams we could estimate an association rate constant (k_{on}) of 3.1×10^3 M^{-1} s^{-1} and a dissociation rate constant (k_{off}) of 0.011 s^{-1}; from these value we calculated a dissociation constant K_d of 3.5 μM (Table 1). Thus, acetylation of RANTES R47K alone resulted in a decrease of binding affinity by almost 2 orders of magnitude. Both association and dissociation rate constants are affected, suggesting that the acetylation of R47K may have decreased both chemokine-heparin electrostatic attraction and the complex stability. Finally, the derivative acetylated at both positions 44 and 47 ([Ac44−47]RANTES) was also injected on heparinized biosensor flow cells. In that, no signal was observed even at 1.6 μM (Figure 4D), confirming the crucial role of residues R44 and R47 in heparin binding. Furthermore, all mono- and biacetylated RANTES derivatives presented a nativelike CD spectrum (not shown), indicating that the modifications introduced did not perturb the structural stability of the chemokine.

Binding and Functional Response of CCR5 to Acetylated RANTES Mutants. To determine whether the residues involved in the binding of RANTES to GAG were playing a role in its binding to CCR5, we investigated the ability of acetylated RANTES mutants to compete for [^{125}I]MIP-1β binding to a CHO−K1 cell line stably expressing CCR5. As shown in Figure 5A and Table 1, acetylation of any of the three residues (R44K, K45, or R47K), identified as important for GAG binding, did not result in a significant decrease of binding affinity for CCR5. However, acetylation of both R44K and R47K of these residues was characterized by a moderate reduction in the binding affinity of this mutant (5-fold). Substitutions of R44 and R47 by lysine (K44 and K47) did not affect the affinity for CCR5. Neither acetylation of residues R17K, R21K, K25, K55, K56, and R59K, nor the Lys substitution of R17 and R59 resulted in a reduction of binding affinity for CCR5 (Figure 5, panels B and C and

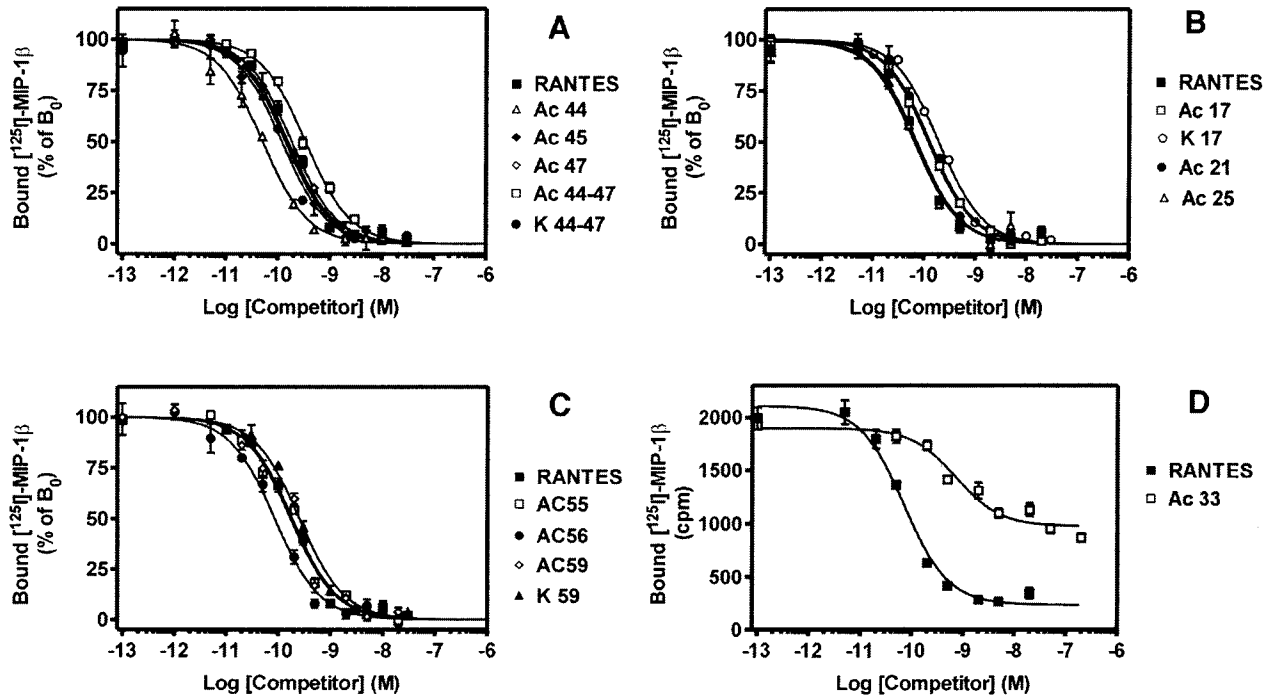

FIGURE 5: Binding of RANTES charge neutralization mutants to CCR5. The different RANTES mutants (A, B, C) were tested for their ability to compete for [^{125}I]-MIP-1β on a CHO−K1 cell line, stably expressing human CCR5 and apoaequorin. The results were analyzed by the GraphPad PRISM software, using a single site-model, and data were normalized for the nonspecific binding (0%) and the specific binding in the absence of competitor (100%). For [Ac33] RANTES (D), nonnormalized data (bound cpm) are presented to illustrate the incomplete competition achieved by this mutant. All points were run in triplicate (error bars: sem). Data are representative of at least two independent experiments.

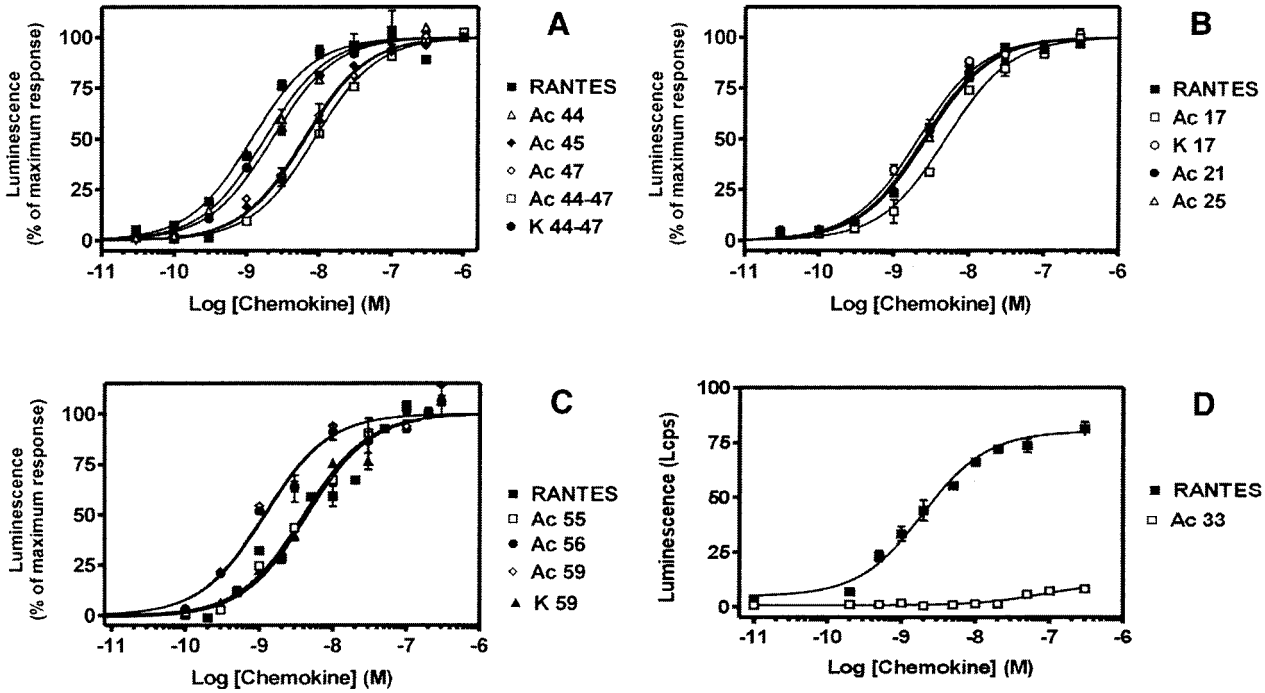

FIGURE 6: Functional response of CCR5 to RANTES charge neutralization mutants. The functional activity of the different RANTES mutants (A, B, C) was assayed by using a cell line coexpressing the receptor together with $G_{\alpha 16}$ and apoaequorin. Light emission resulting from the activation of the apoaequorin-coelenterazine complex was recorded in a luminometer. The results were analyzed by the GraphPad PRISM software, using a sigmoidal dose−response model and the data were normalized for basal (0%) and maximal luminescence (100%). For [Ac33] RANTES (C), nonnormalized data (Lcps) are presented to illustrate the partial activation observed with this mutant. All points were run in triplicates (error bars: sem). Data are representative of at least two independent experiments.

Table 1). However, acetylation of K33 resulted in a strong reduction of the ability of the mutant to compete for [^{125}I]-MIP-1β binding (Figure 5D). The bound tracer was only partially displaced by [Ac33]RANTES (about 50% of wt RANTES): this may reflect the high tendency of this derivative to form aggregates at high concentration, as suggested by the gel filtration experiments. Calculation of the IC_{50} was therefore not accurate in this case, but we could

estimate a decrease of more than one log in binding affinity (Table 1).

The same set of acetylated RANTES mutants was tested for their ability to induce functional responses in CCR5 CHO cells by using a calcium reporter assay as previously described (*26*). As shown in Figure 6A and Table 1, RANTES was characterized by an EC_{50} of 1.73 nM. [Ac44]-RANTES, [Ac45]RANTES, and [Ac47]RANTES, that are characterized by a strong decrease in their ability to bind GAG, stimulated CCR5 with a potency similar to wt RANTES (EC_{50} of 1.4, 2.8, and 4.5 nM for acetylated derivatives at R44K, K45, and R47K, respectively; Figure 6, panels B and C, and Table 1). Doubly acetylated mutant [Ac44−47]RANTES showed a mild (EC_{50} of 23 nM) reduction of its stimulatory activity (Figure 6A). Control double mutant [K44, K47]RANTES presented a potency similar to that of RANTES (EC_{50} of 5 nM, Figure 6A and Table 1), demonstrating that higher EC_{50} observed for [Ac44−47]RANTES is secondary to the neutralization of the positive charges rather than to the change of the side chain of R44 and R47 into lysine. Acetylation of R17K, R21K, K25, K55, K56, and R59K did not change the ability of the mutants to activate CCR5 (Figure 6, panels B and C and Table 1). Acetylation of K33 resulted in a strong impairment of its ability to stimulate CCR5, as small signals only were obtained for concentrations of chemokine higher than 50 nM (Figure 6D). A rough estimate of the EC_{50} (Table 1) indicated a loss of potency of more than one log.

From this set of data, it appears that K33 may be involved in CCR5 binding and activation, in addition to the already reported critical residues of the 20s loop (*28*). Furthermore, it appears that the cluster of basic residues (R44, K45, and R47) in RANTES, that plays a major role in the binding of GAGs, contributes modestly to CCR5 binding and functional response. Thus, reduction in the affinity for GAG did not correlate directly to the reduction in the binding affinity of the mutants to CCR5 and the functional response they elicited.

Binding and Functional Response of CCR1 and CCR3 to RANTES Mutants Acetylated at the 40s Residues. We then investigated if acetylation of RANTES 40s loop residues, which profoundly affects heparin binding, could modify the binding and functional properties toward CCR1 and CCR3, two other receptors for RANTES. In contrast to the situation for CCR5, it was found that acetylation of R47 only decreased the EC_{50} by over 10-fold for CCR1 (164 ± 49 nM, Figure 7A) as compared to wild-type RANTES (12 ± 4 nM). The effect was similar for CCR3 (data not shown). Acetylation of R44 had only moderate effects by itself, and the combined mutation of R44 and R47 did not affect further the functional properties as compared to [Ac47]RANTES alone. These effects were attributed to the neutralization of the charge of the side chain, as [K44, K47]RANTES had wild-type potencies on both receptors. Binding assays demonstrated that the decreased potency of mutant chemokines was the result of impaired affinity for the receptors (Figure 7B).

RANTES Binding and Functional Response of CCR5 CHO Cells Treated by Glycosidases. To determine the importance of cell surface glycosaminoglycans in the binding and the functional response of CCR5 to RANTES, we investigated the effect of enzymatic removal of the different cell surface

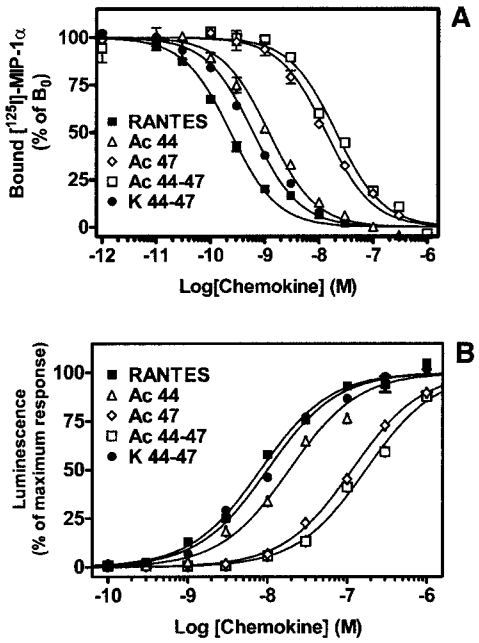

FIGURE 7: Role of charged 40's loop residues on CCR1 binding and functional response. (A) The functional activity of the different RANTES mutants was assayed by using the aequorin assay and a cell line CCR1. The data were normalized for basal (0%) and maximal luminescence (100%). All points were run in triplicates (error bars: sem). Data are representative of at least two independent experiments. (B) RANTES mutants were tested for their ability to compete for [^{125}I]MIP-1α on a CHO−K1 cell line, stably expressing human CCR1. Data were normalized for the nonspecific binding (0%) and the specific binding in the absence of competitor (100%). All points were run in triplicate (error bars: sem). Data are representative of at least two independent experiments.

GAGs by glycosidases on the ability of RANTES to compete for [^{125}I]MIP-1β and to induce functional response in CHO cells expressing CCR5. CHO K1 cells express various GAGs that are able to bind immobilized RANTES (*29*, and data not shown). Bacterial polysaccharide lyases are enzymes with well characterized specificities for GAGs. Heparinase cleaves the (1−4) linkage between *N*-sulfated glucosamine and 2-O-sulfated iduronic acid of heparin (*30*). Heparitinase I cleaves the (1−4) linkages between *N*-acetylated or *N*-sulfated glucosamine and glucoronic acid (*31*, *32*) of heparan sulfate, and chondroitinase ABC cleaves the linkage between *N*-acetyl-galactosamine and D-glucuronic or L-iduronic acids of chondroitin sulfate and dermatan sulfate.

As shown in Figure 8A, all cell surface heparan-sulfate of CHO cells measured by FACS analysis using a specific monoclonal antibody, was totally removed by incubation with heparitinase I whereas chondroitinase ABC had no effect. Treatment of CCR5 expressing CHO cells with heparinase, heparitinase I, and chondroitinase ABC alone, or in combination, did not result either in a reduction of the ability of RANTES to compete for [^{125}I]MIP-1β binding (Figure 8B and data not shown) or in its ability to induce a functional response (Figure 8C and data not shown). These results suggested that cell surface GAGs were not necessary for the high affinity binding of RANTES to CCR5 nor for the Ca^{2+} signaling resulting from this interaction.

Effect of Soluble GAGs on RANTES Binding and Functional Response to CCR5. The absence of direct correlation between the affinities of RANTES acetylated mutants for GAG and CCR5 binding led us to investigate whether the

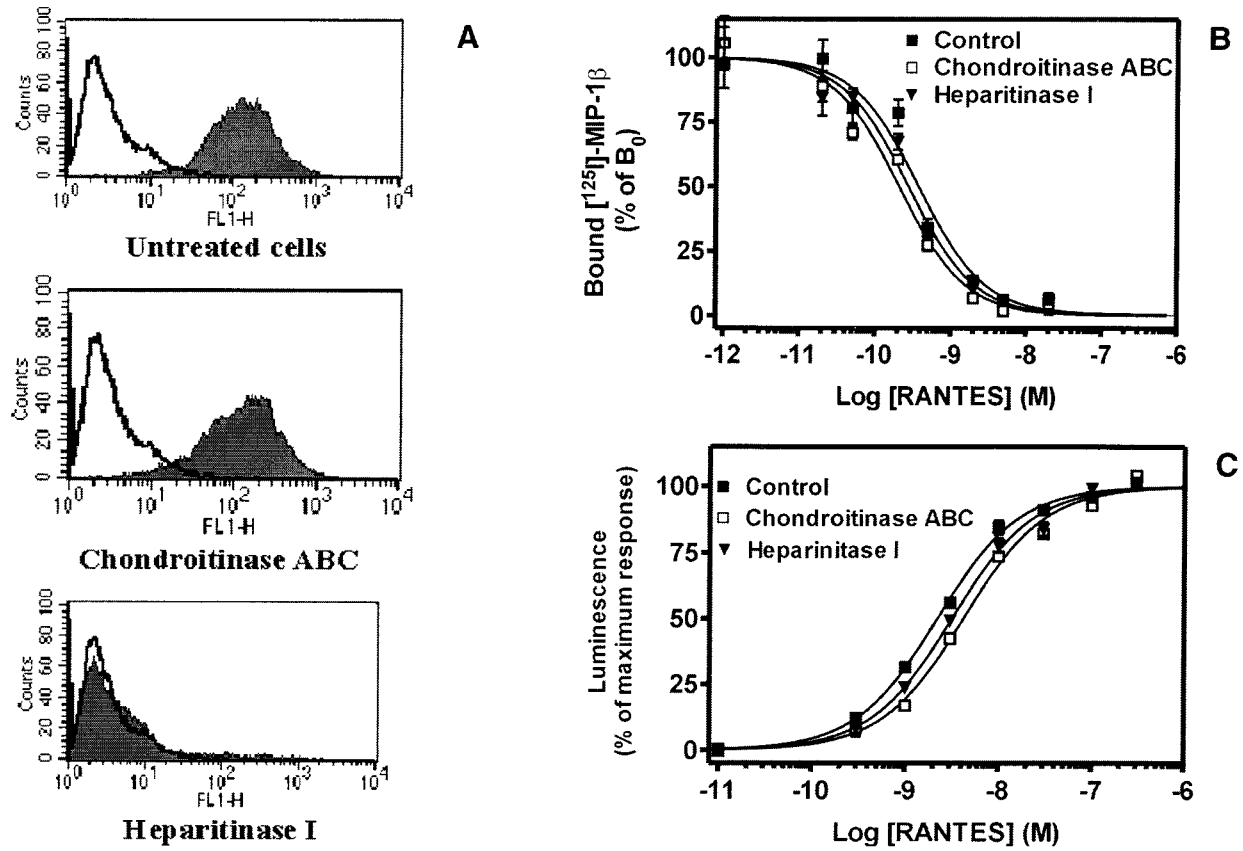

FIGURE 8: Effect of enzymatic removal of cell surface GAGs on RANTES binding and functional response of CCR5. (A) Cell surface expression of heparan-sulfate was analyzed by FACS using an anti-heparan sulfate mAb. Untreated cells or cells incubated with chondroitinase ABC or heparitinase I for 1 h at 37 °C were assayed for heparan-sulfate expression. Cells incubated with secondary antibody only were used as negative control (unfilled histogram). These experiments were performed twice. (B) RANTES binding and (C) functional response of CCR5 expressing cells treated with various glycosidases and assayed for RANTES binding using [^{125}I]MIP-1β as tracer, and functional response to RANTES using aequorin assay. Data are presented as described for Figures 5 and 6. All experiments were run in triplicate (error bars: sem) and data are representative of least two independent determinations.

Table 2: IC_{50} of Inhibition of RANTES Binding to CCR5 by Soluble GAGs[a]

glycosaminoglycan	IC_{50} (μg/mL) $\pm$ sem
Heparin	2.2 $\pm$ 0.8
Heparan sulfate	24.3 $\pm$ 7.8
Chondroitin sulfate C	167 $\pm$ 43.8
Chondroitin sulfate A	175 $\pm$ 75

[a] IC_{50} were obtained from competition binding experiments, using 0.1 nM of [^{125}I]RANTES as tracer (as displayed in Figure 9A). Values represent the mean (μg/mL) and sem of two different determinations.

binding site of RANTES for GAGs and for CCR5 were spatially distinct or overlapping. As shown in Figure 9A, soluble GAGs inhibited the binding [^{125}I]RANTES to CCR5 with a rank of potency similar to that found for the binding of RANTES to immobilized heparin (Table 1 and Figure 3B). Heparin was the most potent GAG inhibitor of [^{125}I]-RANTES binding to CCR5 with an IC_{50} of 2.2 μg/mL, whereas the IC_{50} of heparan sulfate was about 10-fold higher (24.3 μg/mL). Chondroitin sulfate C and A were about 100 fold less potent with an IC_{50} of 167 and 175 μg/mL, respectively (Table 2).

We next investigated the importance of the competitive effect of soluble GAGs on the functional response induced by RANTES on the CHO cell line, expressing CCR5. As shown in Figure 9B, more than 50% of the functional response induced by 10 nM RANTES was antagonized by 0.1 μg/mL heparin. As for competition binding experiments, heparan sulfate and chondroitin sulfates were less potent than heparin, inhibiting more than 50% of the functional response to RANTES only at 10 and 100 μg/mL, respectively (Figure 9B). To test whether the inhibitory effect of soluble GAGs on RANTES induced signaling was secondary to the formation of a GAG-RANTES complex, we tested the effect of soluble GAGs on the functional response induced by the [Ac44−47]RANTES mutant that could no longer bind GAG or by various agents that promote intracellular calcium signaling in CHO cells. Addition of soluble GAGs had no effect on the response mediated by 100 nM [Ac44−47]RANTES, 100 nM CCK, 10 μM ATP, or 0.1% Triton X-100, demonstrating that this inhibitory effect is linked to the ability of GAG to bind RANTES (Figure 9D and data not shown). At high concentrations RANTES is known to form high molecular mass aggregates and GAGs promote this self-aggregation process (*13*). To test whether, in addition to the overlapping binding site of RANTES for GAGs and CCR5, RANTES aggregation could also play a role in the inhibition of RANTES induced signaling by soluble GAGs, we analyzed the effect of soluble GAGs on the functional response of the cell line to a biologically active [E66A]RANTES mutant that presents a reduced tendency to self-associate (*30*). As shown in Figure 9C, a higher concentration of heparin was required to achieve comparable inhibition of the functional response to [E66A]RANTES than

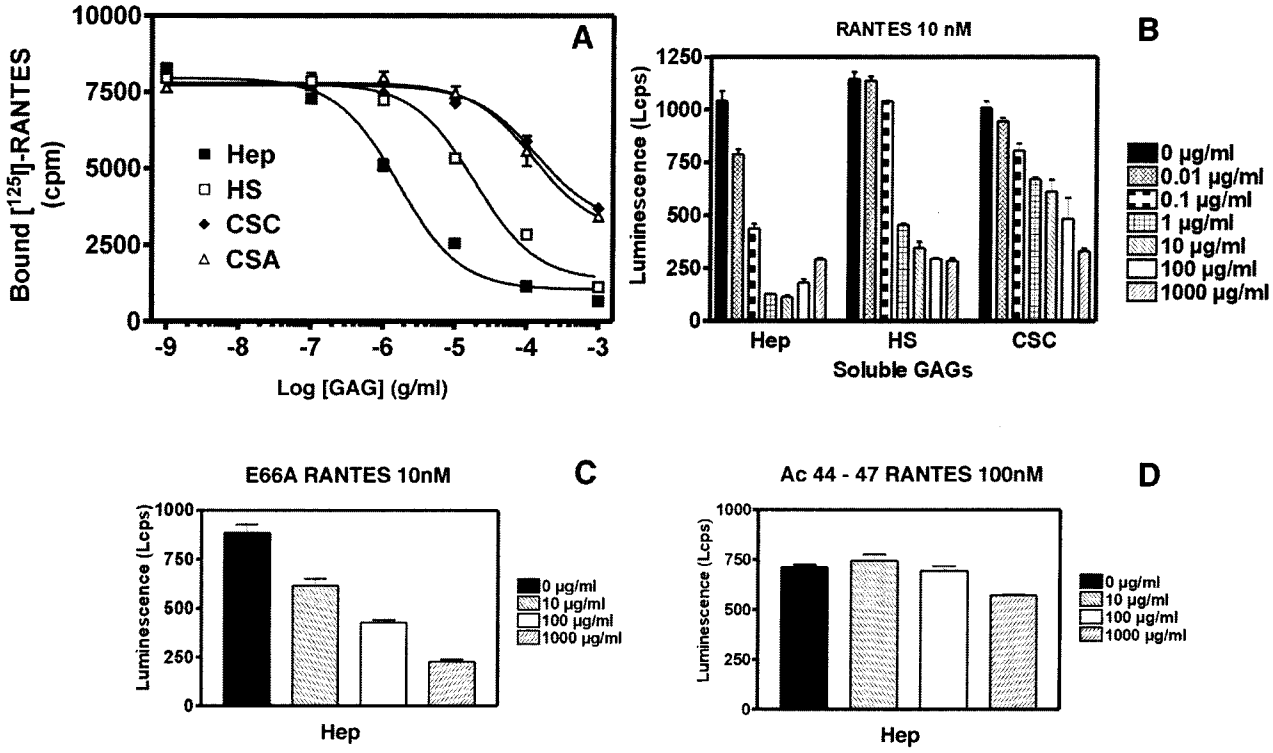

FIGURE 9: Inhibition of RANTES binding and signaling by soluble GAGs. (A) CCR5 expressing cells were assayed for their ability to bind [^{125}I]RANTES in the presence of different concentration of heparin (Hep), heparan sulfate (HS), chondroitin sulfate C (CSC), and chondroitin sulfate A (CSA). Inhibition of RANTES binding was analyzed by nonlinear regression applied to a one-site model using the Graph-Pad PRISM software. All points were run in triplicates (error bars: sem) and experiments were repeated twice. (B) CCR5 expressing cells were assayed for their ability to respond to different agonists in the presence of different concentrations of heparin (Hep), heparan-sulfate (HS), chondroitin sulfate C (CSC), and chondroitin sulfate A (CSA) using aequorin assay. Luminescence in response to 10 nM RANTES, 10 nM [E66A] RANTES, or 50 nM [Ac44−47] RANTES was measured in a luminometer for 30 s in the presence of increasing concentration of GAGs. All points were run in triplicate (error bars: sem) and experiments were repeated at least twice.

of that to wt RANTES. As for heparin, a higher concentration of HS, CSC, and CSA were also required to antagonize the functional response to [E66A] RANTES (data not shown). These results, together with the reduced tendency to aggregation shown by [Ac44−47]RANTES, suggested that two distinct mechanisms may account for the ability of soluble GAGs to inhibit the biological activity of RANTES to CCR5: competition by GAGs to one of the CCR5 binding sites of RANTES and enhanced formation of RANTES aggregates that result in a reduction of the free active chemokine concentration.

DISCUSSION

Protein−GAG interaction is believed to be dominated by electrostatic interactions of the side chains of protein basic residues with the sulfate and carboxylate functions of GAGs. RANTES is high positively charged (5 Lys, 5 Arg, 1 Asp, and 4 Glu) with a net charge of +5 at neutral pH (Figure 1). On the contrary, the homologous CC chemokine MIP-1α presents a −1 overall charge, and MIP-1β is neutral. The highly positive charge density of RANTES may contribute to strengthen the chemokine interaction with negatively charged, highly sulfated GAGs and may predict a strong and tight RANTES−GAG interaction. Indeed, optical biosensor experiments confirmed that RANTES binds heparin with high affinity and exhibits a dissociation constant (K_d) of 32.1 nM. This value is significantly lower than that determined by equilibrium binding of RANTES to Sepharose-immobilized heparin (K_d = 1.8 μM) (*13*, *17*), and may reflect the different methodology used (*33*). RANTES−heparin complexes dissociate at a rather slow rate, requiring 7 min for half-dissociation, suggesting the presence of strong and complementary interactions in this complex. Saturation experiments performed on biosensor chips indicate that RANTES can bind 3.5 saccharide units per RANTES monomer (7−8 saccharide units per dimer). These data are suggestive of an intimate RANTES−GAG interaction, with a high density of chemokine per polysaccharide chain. SDF-1α and Il-8 have been reported to bind 6 or 4−5 saccharide units per chemokine monomer (*17*, *24*), respectively. The higher density of RANTES protein per saccharide unit may indicate that RANTES may bind GAGs as a dimer or tetramer, and may be responsible of protein−protein interaction and aggregation phenomena, as reported in other studies (*27*).

In competitive binding experiments performed on optical biosensor surfaces, RANTES revealed a net selectivity for different GAGs, commonly present on cell surfaces: affinity varies with the following ranking order: heparin > heparan sulfate = chondroitin sulfate C > dermatan sulfate > chondroitin sulfate A. Affinity for different GAGs is quite variable, and RANTES binds heparin with about a 1000-fold higher affinity than chondroitin sulfate A. Thus, RANTES exhibits a marked selectivity for different GAG structures. Heparin (Hep) and heparan sulfate (HS) are highly sulfated GAGs, with the repeated disaccharide unit formed by hexuronic acid (either α-L-iduronic acid or its epimer β-D-glucuronic acid) linked β1−4 to D-glucosamine. Interestingly,

chondroitin sulfate A and C (CSA and CSC) or dermatan sulfate (DS) have the same degree of sulfation with the disaccharide unit formed by a hexuronic acid residue linked β1−3 to *N*-acetyl-β-D-galactosamine; galactosamine can be selectively sulfated at either 4 position in CSA or 6 position in CSC, and hexuronic acid can be either D-glucuronic acid in CSA and CSC or L-iduronic acid in DS. Since RANTES binds 100-fold tighter to CSC than to CSA, it appears that, the different positioning of just one sulfate in CSC vs CSA determines a 100-fold selectivity in binding. This implies that the spatial orientation of particular sulfate and carboxylate groups, and possibly other functional groups in GAG structure, may play a major role in determining the binding affinity of RANTES to GAGs. Thus, both the high affinity and selectivity of RANTES binding to GAGs suggest that electrostatic forces, which are not directional interactions, are just one factor characterizing and reinforcing RANTES−GAG interaction. An optimal steric and energetic complementarity between chemical functions of the polysaccharide structure of GAGs and critical groups of the chemokine molecular surface should better explain the high affinity and selectivity of RANTES−GAGs interaction. The fact that the selectivity that we observed in optical biosensor experiments is confirmed by experiments on cell surface GAGs, and competition with different GAGs in solution, may suggest that this may represent also an important factor of RANTES and chemokine function in vivo (vide infra).

Protein binding sites for heparin contain both arginine and lysine residues, with additional histidine or other residues with H-bonding potential, as evidenced by structural analysis of protein−heparin complexes (*34*−*38*), mutational analyses, and calorimetry titration experiments (*39*). In our study, all five lysine side chains of RANTES were chemically modified, one by one, by acetylation to block their positive charge. Due to the lack of current arginine orthogonal protecting groups, these RANTES residues were singly mutated into lysines, and then individually acetylated. Our data demonstrate that R → K substitution, per se, does not affect RANTES binding affinity to heparin significantly, as demonstrated by binding of control not acetylated R → K mutants on heparinized optical biosensor chips and on CCR5. Analysis of the effect of charge neutralization on heparin binding affinity by optical biosensor technology resulted in a clear identification of the RANTES surface regions responsible for heparin binding. Acetylation of side chains at position 17, 21, 25, 33, 55, 56, and 59 has no effect on heparin binding, while acetylation of residues R44K, K45, and R47K produced a net decrease in heparin binding affinity. Acetylation of R44K and K45 side chains produced a 25-fold decrease in affinity, while acetylation of R47 was more dramatic, and resulted in 100-fold affinity decrease. Thus, blocking the basic residues of RANTES 40s loop produced a reduced affinity for heparin, probably reflecting a destabilized RANTES−heparin complex as the consequence of the loss of a specific ionic interactions. In previous experiments, we attempted to map the heparin-binding site of RANTES by binding tests on heparin-Sepharose columns and elution by sodium chloride gradient. However, we found difficult to quantify the effect of RANTES mutation by this methodology, since the different monoacetylated RANTES derivatives were also eluted to different elution times (different ionic strength) on a simple sulfated hydrophilic matrix, SP−Sepharose, which is assumed to function on the basis of ionic interaction only. Thus, the binding data obtained on heparin-Sepharose column had to be normalized according to the differences in elution time obtained on the ionic exchange column. This was quite a laborious procedure, not devoid of ambiguity. In contrast, technology based on surface plasmon resonance did not require elution by salt, but relies on RANTES intrinsic affinity to heparin and data obtained by this method were unambiguous.

In RANTES structure (Figure 1B), the side chains of basic residues are exposed to solvent and distributed all over the chemokine molecular surface. However, representation of surface electrostatic potential of RANTES (Figure 1C) identifies two major positive regions, one centered about residues R44, K45, and R47 and a second about residues K55, K56, and R59, at the C-terminal end. The first region, spanning the 40s loop, corresponds to the region that we have identified as the heparin-binding domain. The second corresponds to the C-terminal helix region, which has been identified as heparin binding domain in Il-8 (*16*, *17*), PF-4 (*18*) MCP-1 (*19*). In contrast to our conclusions, previous experiments (*14*), based on competition between heparin and a monoclonal antibody mapped to RANTES C-terminal helix, led to conclude that this chemokine could use the C-terminal helix to bind GAGs. However, the antibody epitope was mapped by showing that C-terminal truncated RANTES did not bind the antibody. The lack of binding of a monoclonal antibody to a protein fragment is not evidence that the missing portion is part of the antibody epitope: truncation may affect RANTES conformation and thus antibody recognition. On the contrary, our mutagenesis data provide direct evidence that residues R44, K45, and R47 are involved in GAG binding, and that acetylation of K55, K56, and R59K, in the C-terminal helix, do not affect heparin binding at all. Our data are in complete agreement with those reported on the analogous CC chemokines MIP-1α (*20*, *21*) and MIP-1β (*22*), which mapped the heparin binding domain on the 40s loop. While this work was under evaluation for publication, another work dealing with mutagenesis of RANTES 40s and 50s residues was electronically published (*40*): data from this work confirm the involvement of the 40s loop in heparin binding.

RANTES three-dimensional structure has been solved by NMR by two different groups (*41*, *42*): in both structures, R44, K45, and R47 are located in a loop region connecting two β-strands. Their side chains project into the solvent close to each other, and in one structure [pdb code 1hrj (*42*)], the distances between the positively charged N-ϵ and C-ζ atoms of K45, R47 and K45, R44 are, respectively, 4.3 and 7.6 Å (Figure 1B). More recently, the structure of the two derivatives AOP−RANTES and Met-RANTES have been solved to high resolution by X-ray crystallography (*43*). Interestingly, in both structures a sulfate ion, present in the crystallization buffer, is bound to the side chains of R44, K45, and R47. We suggest that this sulfate ion may mimic the sulfate group of heparin in the RANTES−heparin complex and thus may suggest a model of a heparin sulfate group binding to the cluster of the positively charged residues of the 40s loop that we have identified to interact with RANTES. In addition, our heparin binding experiments indicated that residues R18, R21, and R25 are not implicated in heparin binding. Accordingly, the side chains of mutated

R21 and K25 are pointing to opposite direction as compared to R44, K45, and R47, while R17 is too far from R47 (16.7 Å distance between the positively charged C-ζ atoms of R18 and R47). Thus, our study on RANTES together with previous studies on MIP-1α and MIP-1β identify the 40s loop region connecting two β-strands as a new nonhelical heparin-binding motif, which seems to be common to these three CC chemokines.

RANTES and MIP-1β have been reported to bind to GAGs as a tetramer, whereas MIP-1α binds as a dimer (*13*). RANTES appears as a dimer in solution in NMR studies (*41*, *42*) and in the crystal forms (*43*). However, in the structure of RANTES dimer, the side chains of the R44−K45−R47 cluster of the two monomers point to opposite direction, and it is difficult to model a dimer structure binding to the same heparin molecule, without extensive conformational changes. However, comparison of the four independently calculated RANTES structures reveals a significant variability in dimerization surfaces. Thus, while one RANTES monomer can be superposed to the monomer of a different structure with a low RMS deviation (2.0−3.0 Å) for all backbone atoms, the superposition of the second subunit of the dimer is rather poor. This deviation may reflect a real variability in RANTES subunit association. This finding suggests that RANTES may associate to heparin in a dimeric (or tetrameric) structure which is different from that currently available, but is satisfying effective saccharide−chemokine interaction. Given the structural similarity of RANTES with MIP-1β and MIP-1α, similar conclusions may be also applied to these two later CC chemokines.

The cluster of RANTES positively charged residues, identified as heparin binding domain, seems to be only modestly involved in the high affinity binding of the chemokine to cellular CCR5 and in triggering the mobilization of intracellular Ca^{2+}. Neutralization of single charge either of R44K, K45, or R47K does not affect RANTES binding and activation potency through CCR5. Only double acetylated derivative exhibits a reduction in receptor binding and activation function. In contrast, acetylation of K33 alone resulted in a significant reduction of the functional properties of RANTES; however, this effect is difficult to quantify, due to the aggregation tendency of this derivative at high concentration. In RANTES structure, K33 is in close proximity of F12, and its hydrocarbon side chain packs against the phenyl ring, stabilizing the dimer structure (*41*, *42*). The structural proximity of K33 to F12 and the functional effect observed upon acetylation may suggest a role of this residue and particularly its positively charged side chains in CCR5 binding and activation. The observed functional effect of the double acetylation of R44K and R47K may also suggest that the third β-strand of RANTES may also contribute, at least in part, to the CCR5 binding domain. Thus, RANTES may bind to CCR5 by using the 20s loop, the corner between the first and the second β-strands (including K33), and a region close to the third β-strand preceding the C-terminal helix. Mutagenesis experiments are currently being performed to confirm this hypothesis.

However, while RANTES heparin-binding domain (40s loop) is essentially distinct from the CCR5 binding domain (20s loop), the scenario is quite different for CCR1 and CCR3. Residues of the 20s loop have been shown to be involved in CCR1 and CCR3 binding (*28*): our results indicate that also residues of the 40s loop, i.e., R44, K45, R47, are involved in binding these two receptors and inducing a functional response, with R47 playing a dominant role. Thus, in the case of both CCR1 and CCR3, RANTES heparin binding domain largely overlaps receptor binding and activation domains. Thus, it appears that there is no general rule concerning the location of heparin binding and receptor binding sites in chemokines, and their reciprocal positioning. Our data are in complete agreement with those recently published electronically (*40*).

It has been long reported that GAGs play an important role in chemokine function by capturing chemokines in the extracellular matrix and on the surface of endothelial cells, establishing an immobilized chemokine gradient which is responsible for the chemoattraction of leukocytes to the sites of inflammation (*8*, *9*, *13*). Leukocytes are then recruited as a consequence of chemokine receptor expression and activation by chemokines. However, chemokines can bind to cell surface GAGs, even in the absence of specific chemokine receptors expression (*24* and unpublished results), and the high affinity for GAGs exhibited by RANTES may well explain this finding. Recent studies have, however, suggested additional roles of GAGs in chemokine functions, although these studies are often conflicting. For example, the presence of GAGs attached to the cell surface has been reported to increase binding affinity of RANTES to CCR1 (*13*). Enzymatic removal of GAGs from lymphocytes was also reported to abrogate the ability of RANTES to elicit an intracellular Ca^{2+} signal (*16*). In another study (*39*), no effect of cell surface GAGs were found on chemokine binding. In addition, it has also been reported that removal of heparin from the surface of a PM1 T cell line could reduce the antiviral effect of RANTES (*44*) and that heparan sulfate added in solution could potentiate the inhibition by RANTES of monocytes infection by HIV-1 (*11*). In our study, we demonstrated that enzymatic removal of GAGs from the surface of CCR5 expressing CHO cells by different glycosidases (heparinase, heparitinases I, and chondroitinase ABC), either alone or in combination, did not result either in a reduction of the ability of RANTES to bind CCR5 or to induce a functional response. Furthermore, addition of soluble GAGs, e.g., heparin, heparan sulfate chondroitin sulfate A and C, inhibited RANTES binding to CCR5 and Ca^{2+} signaling at concentrations which are compatible with the affinities of RANTES for the different GAGs, as determined in optical biosensor competition experiments. Thus, in our study, the presence of cellular GAGs is not a prerequisite for the physiological action of RANTES mediated by CCR5, and in addition, RANTES−GAG complexes do not play a positive role in receptor binding and activation. On the contrary, our data suggest that RANTES binds to CCR5 in the free state, while the RANTES−GAG complex is not functional. Two possible mechanisms can explain our findings and the apparent inhibitory role of soluble GAGs on RANTES binding and signaling through CCR5. In fact, given the close location of the GAGs binding domain and the CCR5 binding domain, addition of GAGs, at concentrations high enough to bind to the chemokine, may result in complex structures where the presence of bound GAG may interfere with receptor binding and, consequently, Ca^{2+} signaling, by either simple steric hindrance or electrostatic repulsion of the negatively charged bound GAGs with the

negatively charged receptor extracellular domain. Alternatively, added GAGs can change chemokine conformation or induce high molecular mass aggregates, resulting in failure of normal binding to cell surface receptors. In both mechanisms, RANTES−GAG complexes are non functional, and RANTES has to dissociate from the complex to effectively bind and activate the receptor. The fact that truncated forms of RANTES (*45*) which are monomeric (*46*) can bind CCR5 with nativelike affinity and induce receptor internalization (*47*) are consistent with our results. Our results are fundamentally in agreement with very recent results obtained by Ali et al. (*29*). RANTES and MIP-1β showed equal binding affinities for 745-CHO transfectant cell lines, deficient in surface GAGs, and wt CHO cell lines, together with normal Ca^{2+} flux, when stimulated by high concentrations of chemokines. This demonstrates the absence of absolute requirement of GAGs expression for chemokine activity; in addition, high concentrations of soluble GAGs were always inhibitory. A similar inhibitory role of soluble GAGs was also observed in another recent study by Kuschert et al. (*39*): addition of soluble GAGs inhibited binding of Il-8 and MIP-1α to their receptors and Il-8 induced Ca^{2+} mobilization and chemotaxis of neutrophils, with efficacies compatible with the relative affinity of the chemokines for the different GAGs. Furthermore, an SDF-1α mutant, which is unable to bind to heparin, conserves the functional properties of the wt chemokine to bind and signal through CXCR4 (*24*). Likewise, a mutation of MCP-1 that affected drastically GAG binding did not impair its affinity for CCR2b, nor its ability to induce Ca^{2+} flux and chemotaxis of THP-1 monocytic cells.

In addition, an R46A MIP-1α mutant, unable to bind GAGs, binds and activates CCR1 as efficiently as wt MIP-1α (*21*); further, the R46A MIP-1β mutant, which is devoid of affinity for GAGs, induces T lymphocyte chemotaxis as efficiently as wt MIP-1β (*22*). Thus, it appears that for several chemokines, their ability to bind GAGs is not linked to their effectiveness in binding and activating their receptors, and soluble GAGs may inhibit normal chemokine function. The high selectivity of RANTES (this study) and other chemokines (*39*) for specific GAGs might suggest a role of GAGs on the specificity of chemokine action. GAGs present on vascular cell surfaces, basement membranes, and cells of the immune systems may concentrate specific chemokines in vivo where they have to play their physiological roles, therefore balancing the apparent redundancy of chemokines and the promiscuity of their receptors. The molecules we have synthesized in this study may help to investigate this hypothesis. In conclusion, we have identified a nonhelical GAG binding motif, comprising three positively charged side chains positioned in a loop well exposed to solvent (the 40s loop), which seems to be common to RANTES, MIP-1α, MIP-1β chemokines, and is distinct from the C-terminal helical domain detected in earlier studies on chemokines. RANTES binds to several GAGs with different affinities and a strong selectivity: heparin was the most potent GAG followed by heparan sulfate and chondroitin sulfate. The heparin binding site we have identified is located between the second and third β-strands and for the major part distinct from the receptor binding site, which involves the 20s loop but overlaps the CCR1 and CCR3 binding site. We have shown that the presence of cell surface GAGs is not a prerequisite for RANTES function mediated by CCR5, since removal of cellular GAGs by glycosidases does not affect receptor binding or signaling. In addition, soluble GAGs cannot substitute for cellular GAGs, but inhibit the binding and the functional response of RANTES to CCR5 expressing cells. Our results suggest that GAGs expression may affect RANTES function by concentrating the chemokine in particular in vivo compartments, according to the presence of heparin or heparin-like structure which by its high affinity for RANTES can control the concentration and presence of this chemokine in particular biological compartments. Thus, the combined expression of chemokine receptors and specific GAGs may contribute to the specificity of the in vivo physiological functions of chemokines.

ACKNOWLEDGMENT

We are indebited to Dr. G. Batellier (Laboratoire d'enzymologie et biochimie structurales, CNRS, Gif-sur-Yvette, France) for assistance in analytical ultracentrifugation analysis and S. Swillens for helpful discussion.

REFERENCES

1. Rollins, B. (1997) *Blood 90*, 909−928.
2. Baggiolini, M., Dewald, B., and Moser, B. (1997) *Annu. Rev. Immunol. 15*, 675−705.
3. Wells, T. N. C., Power, C. A., and Proudfooot, A. E. I. (1998) *Trends Pharm. Sci. 19*, 376−380.
4. Baggiolini, M. (1998) *Nature 392*, 565−568.
5. Kelner, G. S., Kennedy, J., Bacon, K. B., Kleyensteuber, S., Largaeepad, D. A., Jenkins, N. A., Copeland, Bazan, J. F., Moore, K. W., Schall, T. J., and Zlotnik, A. (1994) *Science 266*, 1395−1399.
6. Bazan, J. F., Bacon, K. B., Hardiman, G., Wang, W., Soo, K., Rossi, D., Greaves, D. R., Zlotnik, A., and Schall, T. J. (1997) *Nature 385*, 640−644.
7. .Cocchi, F., DeVico, A. L., Garzino-Demo, A., Arya, S. K., Gallo, R. C., and Lusso, P. (1995) *Science 270*, 1811−1815.
8. Witt, D. P., and Lander, A. D. (1994) *Curr. Biol. 4*, 394−400.
9. Middleton, J., Neil, S., Wintle, J., Clark-Lewis, J., Moore, H., Lam, C., Auer, M., Hub, E., and Rot, A. (1997) *Cell 91*, 385−395.
10. Esko, J. D., Elgavish, A., Prasthofer, T., Taylor, W. H., and Weinke, J. L. (1986) *J. Biol. Chem. 261*, 15725−15733.
11. Wagner, L., Yang, O. O., Garcia-Zapeda, E. A., Ge, Y., Kalams, S. A., Walker, B. D., Pasternack, M. S., and Luster, A. D. (1998) *Nature 391*, 908−911.
12. Tanaka, Y., Adams, D. H., Hubscher, S., Hirano, H., Siebenlist, U., and Shaw, S. (1993) *Nature 361*, 79−82.
13. Hoogewerf, A. J., Kuschert, G. S., Proudfout, A. E., Borlat, F., Clark-Lewis, J., Power, C. A., and Wells, T. N. (1997) *Biochemistry 36*, 13570−13578.
14. Burns, J. M., Gallo, R. C., DeVico, A. L., and Lewis, G. K. (1998) *J. Exp. Med. 188*, 1917−1927.
15. Jackson, R. L., Busch, S. J., and Cardin, A. D. (1991) *Physiol. Rev. 71*, 481−539.
16. Web, L. M., Ehrengruber, M. U., Clarck-Lewis, J., Baggiolini, M., and Rot, A. (1993) *Proc. Natl. Acad. Sci. U.S.A. 90*, 7158−7162.
17. Kuschert, G. S. V., Hoogewerf, A. J., Proudfoot, A. E. I., Chung, C., Cooke, R. M., Hubbard, R. E., Wells, T. N. C., and Sanderson, P. N. (1998) *Biochemistry 37*, 11193−11201.
18. Maione, T. E., Gray, G. S., Hunt, A. J., and Sharpe, R. J. (1991) *Cancer Res. 51*, 2077−2083.
19. Chakravarty, L., Rogers, L., Quach, T., Breckenridge, S., and Kolattukudy, P. E. (1998) *J. Biol. Chem. 273*, 29641−29647.
20. Graham, G. J., Wilkinson, P. C., Nibbs, R. J. B., Kolset, S. O., Parker, A., Freshney, M. G., Tsang, L. S., and Pragnell, I. B. (1996) *EMBO J. 15*, 6506−6515.

21. Koopmann, W., and Frangel, M. S. (1997) *J. Biol. Chem. 272*, 10103−10109.
22. Koopmann, W., Ediriwickrema, C., and Krangel, M. S. (1999) *J. Immunol. 163*, 2021−2127.
23. Amara, A., Lorthioir, O., Valenzuela, A., Magerus, A., Thelen, M., Montes, M., Virelizier, J. L., Delepierre, M., Baleux, F., Lortat-Jacob, H., and Arenzana-Seisdedos, F. (1999) *J. Biol. Chem. 274*, 23916−23925.
24. Gomez-Martinez, P., Dessolin, M., Guibé, F., and Albericio, F. (1999) *J. Chem. Soc., Perkin Trans. 1*, 2871−2874.
25. Blanpain, C., Migeotte, I., Lee, B., Vakili, J., Doranz, B. J., Govaerts, C., Vassart, G., Doms, R. W., and Parmentier, M. (1999) *Blood 94*, 1899−1905.
26. Blanpain, C., Doranz, B. J., Vakili, J., Rucker, J., Govaerts, C., Baik, S. S. W., Lorthioir, O., Migeotte, I., Libert, F., Baleux, F., Vassart, G., Doms, R. W., and Parmentier, M. (1999) *J. Biol. Chem. 274*, 34719−34727.
27. Czaplewski, L. G., McKeating, J., Craven, C. J., Higgins, L. D., Appay, V., Brown, A., Dudgeon, T., Howard, L. A., Meyers, T., and Owen, J., et al. (1999) *J. Biol. Chem. 274*, 16077−16084.
28. Pakianathan, D. R., Kuta, E. G., Artis, D. R., Skelton, N. J., and Hébert, C. A. (1997) *Biochemistry 36*, 9642−9648.
29. Ali, S., Palmer, A. C. V., Baneiee, B., Frichley, S. J., and Kirby, J. A. (2000) *J. Biol. Chem. 275*, 11722−11727.
30. Linhardt, R. J., Turnbull, J. E., Wang, H. M., Loganathan, D., and Gallagher, J. T. (1990) *Biochemistry 29*, 2611−2617.
31. Yamada, S., Sakamoto, K., Tsuda, H., Yoshida, K., Sugahara, K., Khoo, K. H., Morris, H. R., and Dell, A. (1994) *Glycobiology 4*, 69−78.
32. Sugahara, K., Tohno-oka, R., Yamada, S., Khoo, K. H., Morris, H. R., and Dell, A. (1994) *Glycobiology 4*, 535−44.
33. Karlsson, R., Raos, H., Fägerstam, L., and Person, B. (1994) *Methods Comp. Methods Enzymol. 6*, 99−110.
34. Stukey, J. A., St Charles, R., and Edwards, B. F. P. (1992) *Proteins: Struct., Funct., Genet. 14*, 277−287.
35. Ornitz, D. M., Herr, A. B., Nilsson, M., Westmann, J., Svahn, C. M., and Waksman, G. (1995) *Science 268*, 432−436.
36. Faham, S., Hileman, R. E., Fromm, J. R., Linhardt, R. J., and Rees, D. C. (1996) *Science 271*, 1116−1120.
37. Pineda-Lucena, A., Jimenez, M. A., Lozano, R. M., Nieto, J. L. Santoro, J., Rico, M., and Gimménez-Gallego G. (1996) *J. Mol. Biol. 264*, 162−178.
38. DiGabiele, A. D., Lax, I., Chen, D. I., Svahn, C. M., Jaye, M., Schlessinger, J., and Hendrickson, W. A. (1998) *Nature 393*, 812−817.
39. Kuschert, G. S. V., Coulin, F., Power, C. A., Proudfoot, A. E. I., Hubbard, R. E., Hoogewerf, A. J., and Wells, T. N. C. (1999) *Biochemistry 38*, 12959−12968
40. Proudfoot, A. E. I., Fritchley, S., Borlat, F., Shaw, J. P., Zwahlen, C., Trkola, A., Clapham, P. R., and Wells, T. N. C. (2001) *J. Biol. Chem.* (in press).
41. Skelton, N. J., Aspiras, F., Ogez, J., and Schall, T. J. (1995) *Biochemistry 34*, 5329−5342.
42. Chung, C., Cooke, R. M., Proudfoot, A. E. I., and Wells T. N. C. (1995) *Biochemistry 34*, 3907−3914.
43. Wilken, J., Hoover, D., Thompson, D. A., Barlow, P. N., McSparron, H., Picard, L., Wlodawer, A., Lubkowsi, J., and Kent, S. B. H. (1998) *Chem. Biol. 6*, 43−51.
44. Oravecz, T., Pal, M., Wang, G., Roderiquez, G., Ditto, M., and Norcross, M. A. (1997) *J. Immunol. 159*, 4587−4592.
45. Arenzana-Seidedos, F., Virelizier, J. L., and Rousset, D. (1996) *Nature 383*, 400.
46. Ylistagui, L., Vizzavona, J., Drakopoulou, E., Paindavoine, P., Calvo, C. F., Parmentier, M., Gluckman, J. C., Vita, C., and Benjouad A. (1998) *AIDS 12*, 977−984.
47. Amara, A., Gall, S. L, Schwartz. O., Salamero, J., Montes, M., Loetscher, P., Baggiolini, M., Virelizier, J. L., and Arenzana-Seisdedos, F. (1997) *J. Exp. Med. 186*, 139−146.
48. Koradi, R., Billeter, M., and Wütrich, K. (1996) *J. Mol. Graphics 14*, 51−55.

BI002670N